

Colloidal stability of magnetic nanoparticles in molten salts

By
Vaibhav Somani

B. Tech Materials Science and Engineering
M. Tech Materials Science and Engineering
Indian Institute of Technology, Mumbai, India, 2007

ARCHIVES

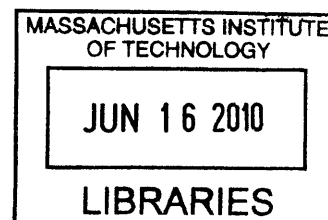
Submitted to the Department of Materials Science and Engineering in partial fulfillment of the requirements for the degree of

Masters of Science in Materials and Science Engineering
at the
MASSACHUSETTS INSTITUTE OF TECHNOLOGY


May 2010

[June 2010]

© 2010 Massachusetts Institute of Technology. All rights reserved.



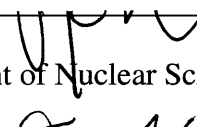
Signature of Author: _____


Vaibhav Somani
Department of Materials and Science Engineering
May, 2010

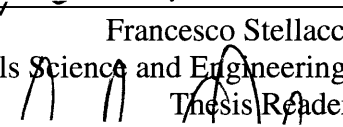
Certified by: _____


T. Alan Hatton
Department of Chemical Engineering
Thesis Advisor

Certified by: _____


Jacopo Buongiorno
Department of Nuclear Science and Engineering
Thesis Advisor

Accepted by: _____


Francesco Stellacci
Department of Materials Science and Engineering
Thesis Reader

Accepted by: _____


Christine Ortiz
Chair, Departmental Committee on Graduate Students

Abstract

Molten salts are important heat transfer fluids used in nuclear, solar and other high temperature engineering systems. Dispersing nanoparticles in molten salts can enhance the heat transfer capabilities of the fluid. High temperature and high ionicity of the medium make it difficult to make a colloidally stable dispersion of nanoparticles in molten salts. The aggregation and sedimentation kinetics of different nanoparticles dispersed in molten salts is studied, and trends of settling rates with system parameters like particle size, temperature and concentration are observed. Finally, a hypothesis based on ultra low values of Hamaker coefficient is suggested in order to achieve long term colloidal stability in molten salts medium.

Acknowledgements

At first, I would like to thank my advisor Prof. T. Alan Hatton for being extremely helpful and supportive throughout the course of this thesis. I would also like to thank Prof. Jacopo Buongiorno for his valuable inputs from time to time, and Prof. Francesco Stellacci for agreeing to be my thesis reader.

Then, I would like to thank Prof. Wai Yim Ching for carrying out the Ab Initio calculations of dielectric spectra of different materials at my request. I will also like to express gratitude to Dr. Thomas McKrell and Stefano Passerini for their valuable help and advice in setting up various experiments. I would also like to acknowledge very valuable help offered by Rick Rajter, Diwakar Shukla, Asha and Vinay over the course of the thesis. Also, I would sincerely like to thank each and every member of the Hatton group, for providing extremely friendly and helpful work atmosphere over the entire course of my stay. I would also like to thank Chesonis Family Foundation and MIT Energy Initiative for funding

Lastly, I would like to express my heartfelt gratitude towards my friends Hitesh, Prithu, Abhinav, Shreerang, Saurabh, Asha, Mehul, Ravi, Vinay, Anusha, Himanshu, Siddharth and Naveen who have made my stay at MIT memorable and pleasurable

Table of Contents

1. Introduction.....	1
1.1 Motivation.....	3
1.1.1 Concentrated Solar Power on Demand.....	4
1.2 Methodology and approach.....	6
1.3 References.....	8
2. Theory of colloidal stability and aggregation kinetics.....	9
2.1 Interactions between particles in a colloidal system.....	9
2.1.1 Electrostatic repulsion.....	9
2.1.2 van der Waals forces.....	15
2.2 DLVO theory of colloidal stability.....	18
2.3 Non DLVO forces: Hydrodynamic effects.....	26
2.4 Smoluchowski model of aggregation kinetics.....	29
2.4.1 Mechanisms of collisions.....	30
2.5 Studies of colloidal stability in Ionic liquids.....	33
2.6 References.....	37
3. Estimation of aggregation kinetics in molten salts by turbidity measurements:	
Experimental results.....	39
3.1. The objective and methodology of experiments.....	39
3.1.1 Selection of salts and nanoparticles.....	40

3.1.2 Method of dispersing nanoparticles in molten salts.....	41
3.1.4 Estimation of settling rates.....	43
3.2 Results and discussion	45
3.2.1 Different salts and particles	45
3.2.2 Turbidity measurement experiments.....	50
3.3 Summary	66
3.4 References	68
4. Potential stabilization of nanoparticle suspensions through ultra-low Hamaker coefficients	69
4.1 Modern theory to estimate Hamaker Coefficient (Lifschitz formulation)	72
4.1.1 The data required for calculation of the Hamaker coefficient using lifschitz formulation.....	73
4.1.2 van der Waals – London dispersion spectra ($\epsilon(i\xi)$)	77
4.1.4 Lifschitz formulation for calculation of Hamaker coefficients.....	86
4.2 Obtaining the ϵ'' spectrum for molten salts.....	87
4.2.1 Experimental options	88
4.2.2 Ab Initio calculation of ϵ'' for molten salts.....	92
4.3 Summary	94
4.4 References.....	95
5. Conclusions and Future Work	96

List of Figures

Figure 1-1: Methods of stabilizing nanoparticles in a suspension. (A) Steric stabilization, (B) Electrostatic stabilization	2
Figure 1-2: The basic model design of CSpond. Solar rays enter directly into the molten salt, where they are absorbed by the dispersed nanoparticles.	5
Figure 2-1: Development of a charge on oxide particles in aqueous medium due to hydroxylation	10
Figure 2-2: Schematic of the electrical double layer (EDL) formed across a negatively charged colloidal particle. Image Source: http://www.nbtc.cornell.edu/facilities/downloads/zetasizer%20chapter%2016.pdf	12
Figure 2-3: The variation of potential with distance between electrodes with different surface charge densities in an ionic liquid cell. The potential profile differs significantly from the exponentially decaying one observed in the case of an electrical double layer. ⁴	14
Figure 2-4: A typical DLVO potential curve. It is the summation of the electrostatic and van der Waals interaction energy, which results in a one maximum and two minima.	20
Figure 2-5: Variation of DLVO energy barrier with increasing salt concentration. As the salt concentration increases, the energy barrier decreases due to the screening of electrostatic interactions	22
Figure 2-6: Effect of charge screening ¹⁵ by ionic liquids on the energy barrier	23
Figure 2-7: Variation of stability ratio with salt concentration. The stability ratio initially decreases linearly with increasing salt concentration, and becomes constant after reaching the critical concentration.....	24

Figure 2-8: Variation of limiting stability ratio versus the Hamaker coefficient taking into consideration the hydrodynamic interactions (Solid line). The dotted line shows the variation when hydrodynamic interactions are not considered..... 28

Figure 2-9: Comparison of settling rates of titania nanoparticles in pure water and water saturated with NaCl. The vial on the left is the one with pure water. The snapshots were taken instantaneously after sonication (A), after 20 minutes (B), after 120 minutes (C) and after 8 hours (D). The nanoparticles aggregate and settle in the salt solution at a much higher rate 35

Figure 3-1: Experimental set up for dispersing the nanoparticles in molten salts. 42

Figure 3-2: Experimental set up used to measure turbidity of suspensions over a period of time. A Laser pointer was used as the light source and a spectrometer was used to measure the intensity of received light. Measurements were taken at periodic intervals of time..... 43

Figure 3-3: Settling of 0.1 wt% titania nanoparticles in molten sodium nitrate at 350 °C. 46

Figure 3-4: Settling of 0.1 wt% silica nanoparticles in sodium nitrate AT 350 °C. The aggregation is seemingly faster than that of titania in molten nitrate and large clusters float around in the salt. 47

Figure 3-5: Settling of 0.1 wt% alumina nanoparticles in molten sodium nitrate salt at 350 °C.. 47

Figure 3-6: Settling of 0.1 wt% silica particles in NaCl-KCl mixture at 750 °C. The turbidity caused by silica particles in chloride salt is very high compared to that of silica particles in nitrate salt. Also, large floating clusters of silica seen in nitrate are not seen in chloride. 49

Figure 3-7: Variation of the transmitted intensity with time for a suspension of titania nanoparticles in molten sodium nitrate at 350 °C. Initially, there is no signal due to the high turbidity of the suspension. Once the signal is obtained, it varies linearly with time, until the turbidity is low enough that the receiver saturates..... 51

Figure 3-8: Variation of transmitted intensity with time of molten sodium nitrate with suspended alumina nanoparticles at 350 °C. The trend is very similar to that for titania nanoparticles but the attenuation caused by alumina nanoparticles is far less than that caused by titania nanoparticles. 51

Figure 3-9: Variation of turbidity with time of a suspension of titania nanoparticles in molten sodium nitrate. The turbidity sees an exponential decay with time. 53

Figure 3-10: Evolution of attenuation area with time in a colloidal system aggregating due to Brownian collisions. The area under the lognormal curve at a given time represents the total attenuation area at that time. 55

Figure 3-11: The decrease in attenuation area (or the turbidity) as a function of time, obtained by plotting the area under each curve in Figure 3-10 56

Figure 3-12: Expected variation in transmitted light with time during Brownian motion dominated aggregation. Most of the aggregation due to Brownian motion happens in the first few minutes. 57

Figure 3-13: Transmitted intensity vs time for titania nanoparticles dispersed in molten sodium nitrate at three different temperatures. The threshold value for signal decreases and the slope of the linear regime increases with temperature. There is a significant variation (increase) in the total aggregation rate with temperature. 58

Figure 3-14: Effect of temperature gradient on aggregation of nanoparticles. The nanoparticles aggregated close to the hotter end. 61

Figure 3-15: Transmitted intensity Vs time curves for different sized titania nanoparticles in molten sodium nitrate at 350 °C. There seems to be no significant effect on the aggregation rate with the change in particle size. 62

Figure 3-16: Transmitted intensity Vs time (A), and turbidity vs time (B) curves for titania nanoparticles in molten sodium nitrate at 350 °C for two different concentrations. 64

Figure 3-17: Effect of different media on the sedimentation rates of nanoparitcles. The high temperature chloride suspension reached the threshold value before the nitrate but ended up taking more time to reach detector saturation point..... 66

Figure 4-1: An example of conversion of absorption spectrum to van der Waals spectrum through Kramers Kronig transformation. At the top, we have the ϵ'' of solid KCl, and at the bottom, we have a converted smooth monotonic van der Waals spectrum. 78

Figure 4-2: Illustration of calculation of the Hamaker coefficient using the van der Waals spectra of the materials of interest. Note that the vertical lines represent the Matsubara frequencies, over which the summation has to be carried out..... 80

Figure 4-3: Effect of ϵ'' peak intensity on vdW-Lds. As the peak intensity increases, the vdW-Lds shifts upwards. 82

Figure 4-4: Variation of vdW-Lds with ϵ'' peak position. The vdW-Lds flattens out as the ϵ'' peak moves towards right. 83

Figure 4-5: Effect of ϵ'' peak width on vdW-Lds with constant peak position and area under the peak 84

Figure 4-6: The ϵ'' and vdW-Lds spectra of two hypothetical materials, with significantly different absorption properties but very close vdW-Lds 85

Figure 4-7: Ellisometric set up for CaF₂ melt at 1823K. 88

Figure 4-8: The approximated vdW spectra for molten KCl obtained by scaling the ϵ'' spectrum of solid KCl before performing KK transformation. 90

Figure 4-9: Variation of Hamaker coefficient with particle separation for SiO₂-KCl-SiO₂ system.
The decreasing value of the Hamaker coefficient with the distance is due to retardation..... 91

Figure 4-10: The ϵ'' , n and vdW-Lds spectra of molten KCl at 1000°C obtained by Ab Initio
calculations using a 3X3 KCl supercell cooked up at 1000 °C..... 93

Figure 5-1: Core Shell nanoparticles can provide both strong absorption and colloidal stability 98

List of Tables

Table 3-1: Estimation of Hamaker coefficient of different nanoparticles in molten sodium nitrate and molten NaCl and KCl mixture 45

Table 3-2: Variation of viscosity, density and perikinetiic collision constant in NaNO₃ with temperature. 59

1. Introduction

Nanofluids are stable colloidal suspensions of nanoparticles in a base fluid medium. The sizes of the particles dispersed in the liquid medium are typically less than 100 nm. These colloidal dispersions of ultra small particles are being studied the world over as advanced heat transfer fluids for various applications such as microelectronics, nuclear systems, fuel cells, hybrid powered engines etc.¹ It has been observed that the heat transfer coefficient in nanofluids is significantly higher than that of the base fluid.² The exact reasons leading to this increase in heat transfer coefficient has been a subject of great debate.³

For nanofluids to possess these superior heat transfer properties, it is important that the nanoparticles remain colloidally suspended in the medium, and do not aggregate and sediment out. In the absence of repulsive forces between them, collisions between particles undergoing random Brownian motion leads to their sticking to one another due to the van der Waals forces of attraction between them. Also, aggregation is preferred from point of view of energetics because nanoparticles tend to minimize their surface free energy by forming large aggregates. There are two main methods of providing colloidal stability to nanoparticles in a liquid medium. Firstly, if the surface of the particles is charged, then the particles repel each other on approach, thereby avoiding aggregation. In the second method, long polymeric surfactants are attached to the surface of the particles, which hinder their approach sterically and keep them stable in suspension. These two most commonly used techniques to achieve colloidal stability are shown in Figure 1-1.

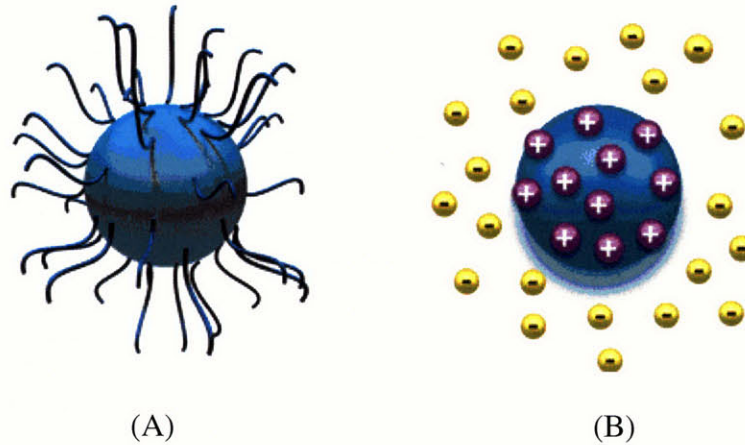


Figure 1-1: Methods of stabilizing nanoparticles in a suspension. (A) Steric stabilization, (B) Electrostatic stabilization

It must be noted that the colloidal stability is dependent on various system parameters including materials involved (both particles and medium), particle size, temperature and chemistry, as all of these influence the aggregation of particles in some way or the other. Some systems may naturally lead to charges on the surfaces of the particles and be stable without the need for any external stabilization, while others require one of the two stabilization techniques mentioned above. In this work, we intend to study the aggregation behavior of nanoparticles in molten salts at high temperatures. We will evaluate the impact each of the system parameters makes on the aggregation kinetics of the nanoparticles and investigate the possibility of making colloiddally stable molten salt nanofluids in this medium. We will begin by looking into the motivation for this study and discuss some of the potential applications of high temperature molten salt nanofluids.

1.1 Motivation

The particular media that we are interested in are high melting temperature inorganic salts such as alkali halides (NaCl, KCl, LiCl etc.) and alkali nitrates (NaNO₃, KNO₃ etc). Molten salts are very useful high temperature heat transfer fluids as they stay at low vapour pressures even at extremely high temperatures, thereby eliminating the need to pressurize the system. In addition, these salts are relatively low cost, are thermodynamically stable, and have high heat capacities. Consequently, molten salts, usually in the form of mixtures, are used extensively as coolants in nuclear reactors and concentrated solar thermal power plants. Nitrate salts are most often used, with the operating temperatures in the range of 250 - 550 °C. The peak temperatures are limited by the chemical decomposition of the nitrate salts.

The use of chloride salts, which are stable at much higher temperatures as compared to nitrate salts, is desirable in solar thermal systems, nuclear reactors and many other high temperature engineering systems. These plants require intermediate heat transfer loops that connect the energy source to the power cycle. The heat-to-electricity efficiency increases with increasing temperatures. As such, there are large economic and environmental incentives to increase peak temperatures in these systems from the existing levels. Today, the highest-temperature commercial heat transfer fluids are nitrate salts used in various chemical plants and solar thermal power plants. The peak temperatures are between 550 and 600°C and are limited by the chemical decomposition of the nitrate salts. Higher-temperature salts made of fluorides, chlorides, and carbonates are being developed as coolants in solar power towers, nuclear reactors (advanced high-temperature reactor, molten salt reactor, salt-cooled fast reactors), and various intermediate heat transfer loops. These salts are thermodynamically stable, operate at low pressures, have high

heat capacities, and are transparent over much of the visible spectrum. While the salts have relatively low costs, the materials of construction for operations between 600 and 1000°C are expensive. The practicality of these higher-temperature systems depends partly upon efficient heat transfer that minimizes the size of heat exchangers and other equipment made of expensive materials.

Nanoparticles dispersed in molten salts can significantly alter their heat transport efficiency, as they do for any other fluid. Furthermore, at high temperatures at which molten salts operate, radiation heat transport becomes important because it depends upon the temperature to the fourth power. Nanoparticles introduced in the molten salt can conductively absorb heat from the fluid and radiate it to heat transfer surfaces. The general importance of nanoparticles in terms of heat transfer is recognized from traditional studies of particles in high-temperature combustion systems. One particular example of an application in which a dispersion of nanoparticles in molten salts can be used for efficient heat absorption and storage is the ‘Concentrated Solar Power on Demand (CSpond) project, described briefly below.

1.1.1 Concentrated Solar Power on Demand

In traditional solar thermal power plants, a molten salt flows through metallic pipes. Concentrated solar rays are used to heat up the metallic pipes, which in turn transfer the heat to the salt that flows through them. The peak temperatures, as stated above, are limited by the decomposition of nitrate salts. This design has many built in inefficiencies, the major one being heat loss from non-insulated metallic pipes to the surroundings.

CSpond proposes a much more efficient design, wherein concentrated solar power will be used directly to heat up the salt, which will be maintained in a molten state in a thermally insulated tank, as shown in Figure 1-2. The molten salt can then be used as a heat storage and heat transfer fluid. Now, molten salts are usually semi-transparent and hence will not be able to absorb radiation significantly in the visible region; this is where dispersed nanoparticles can play an important role. The nanoparticles can absorb the solar energy in the visible region, and then transfer the heat to the molten salt by conduction and convection. This will result in the heat being absorbed over the entire volume of molten salts, and the heat from the otherwise wasted visible part of the solar spectrum would be utilized efficiently.

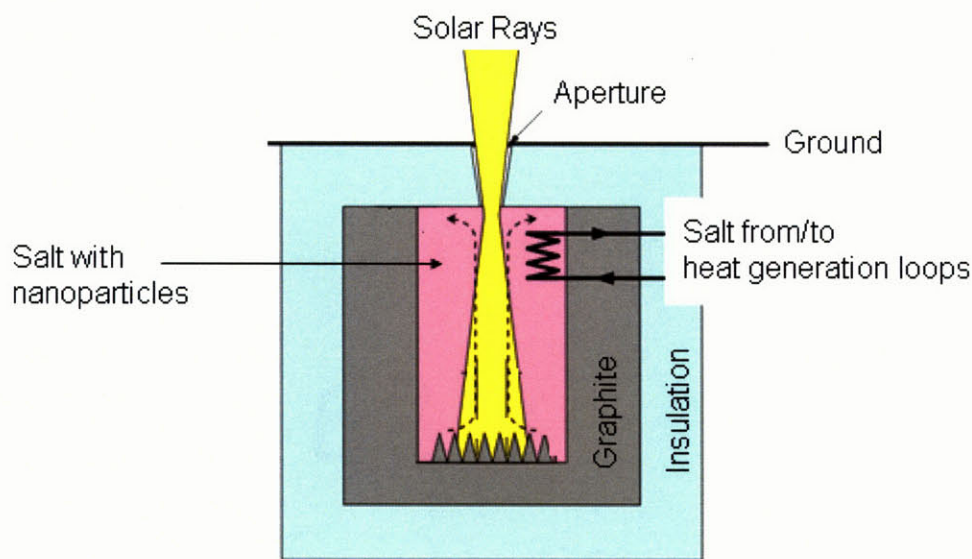


Figure 1-2: The basic model design of CSpond. Solar rays enter directly into the molten salt, where they are absorbed by the dispersed nanoparticles.

Sandia laboratories have studied the effect of nanoparticles on absorptivity of molten salts, and found that 0.1 wt% of nanoparticle dopants can enhance solar energy absorbed per centimetre of fluid depth from 8% to 90%.⁴ Thus, the utility of dispersed nanoparticles in molten salts has been

established. However, to the best of our knowledge, no attempt has ever been made to study aggregation propensity and colloidal stability of nanoparticles in molten salts. It is important to realize that for any engineering benefit to be gained by exploiting the use of nanoparticles in molten salts, the problem of colloidal stability is of utmost importance. Besides, even if particles are not intentionally added, they can be present (or generated) in the system as impurities, and it is important to understand their colloidal stability to determine the potential impact of such impurities on the heat transfer properties of the salt.

1.2 Methodology and approach

As stated above, the goal of this project is to study the colloidal stability of various nanoparticles in the molten salt medium and evaluate the possibility of developing kinetically stable nanofluids in these environments. Because of the high temperatures ($\sim 1000^{\circ}\text{C}$) and high thermal energy, the requirements for engineered nanoparticles in these systems are more severe than are those for nanoparticles in lower temperature fluids. However, before moving into the main problem of colloidal stability, we need to bear in mind a few other constraints that limit our choices of nanoparticles that could be appropriate for this high temperature system. Firstly, it needs to be ensured that the nanoparticles are physically and chemically stable in the medium. For physical stability, one needs to choose particles that won't soften and deform at temperatures in the range of 1000°C . Thus, only high melting point ceramics can be considered. Also, for chemical stability, it needs to be ensured that the nanoparticles do not react chemically with the molten salts at the temperatures of interest. Furthermore, the nanoparticles also need to be extremely insoluble in the salt medium in order to avoid particle coarsening due to Ostwald ripening. Few candidate materials that satisfy this criterion are high temperature ceramics such as silica (M.P.

1650 °C), alumina (M.P.2072 °C), titania (M.P. 1843°C), etc. In fact, these are the most common materials used for most high temperature applications.

Now, this leaves us with our main problem of colloidal stability. In order to evaluate the potential development of dispersed nanoparticles that can provide strong thermal absorption and radiant emission for enhancement of heat transfer rates within molten salts, we will have to study the colloidal behaviour of the nanoparticles in this medium in some detail. Both low temperature nitrate salts (250-550 °C) and high temperature chloride salts (550-1000 °C) will have to be considered. We will first begin by looking into the fundamentals of particle aggregation and deposition in a general colloidal system, and understand in detail the processes and parameters that determine the colloidal stability in any dispersion. We will look into the peculiarities of our medium (high temperature, ionicity etc) that introduces difficulties in obtaining a stable dispersion of nanoparticles, and evaluate the parameters that we expect would theoretically make an impact on colloidal stability. We will then experimentally study the rate of deposition of nanoparticles in molten salts, and its variation with important parameters such as materials, temperature, concentration etc. Finally, based on the theory and experimental observations, we will evaluate the possibility of engineering a system which can remain colloidally stable.

1.3 References

1. Das, S., Nanofluids: Science and Technology. Wiley Interscience: 2007; p 397.
2. Kakac, S.; Pramuanjaroenkij, A., Review of convective heat transfer enhancement with nanofluids. International Journal Of Heat And Mass Transfer 2009, 52, (13-14), 3187-3196.
3. Buongiorno, J., Convective transport in nanofluids. Journal of Heat Transfer (American Society of Mechanical Engineers) 2006, 128, (3), 240.
4. Drotning, W. D., Optical-Properties Of Solar-Absorbing Oxide Particles Suspended In A Molten-Salt Heat-Transfer Fluid. Solar Energy 1978, 20, (4), 313-319.

2. Theory of colloidal stability and aggregation kinetics

2.1 Interactions between particles in a colloidal system

The interaction forces between the particles that are primarily responsible for the behavior of the colloidal systems, in particular, their colloidal stability, are usually those of electrostatic repulsion and van der Waals attraction. In addition, hydration and steric forces can also come into play in the system and make a significant impact on colloidal stability. We describe briefly the origin and the impact of each of the forces in the system of our interest in this section.

2.1.1 Electrostatic repulsion

In many colloidal systems, repulsive electrostatic interactions between the particles play the most important role in providing colloidal stability to the particle suspension. If the colloidal particles are charged, they tend to repel one another and prevent particle aggregation (and eventual sedimentation), thereby ensuring colloidal stability. Many particles naturally develop a charged surface in a particular medium. There can be several origins of such a charge on the surface, one example being that of metal oxides like SiO_2 , Al_2O_3 , TiO_2 , Fe_2O_3 etc. in an aqueous medium. In contact with water, the oxide surface becomes hydroxylated, thereby resulting in either positive or negative surface charge, depending on the pH. The ionization of such groups can be represented as shown in Figure 2-1.

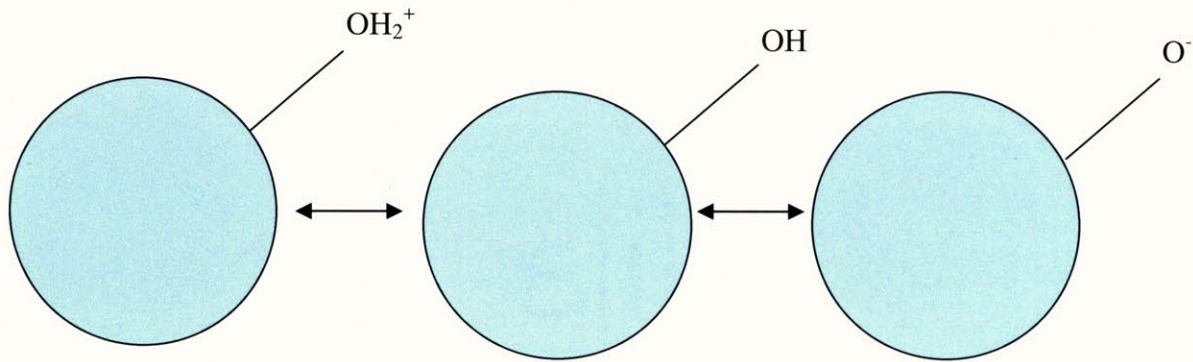


Figure 2-1: Development of a charge on oxide particles in aqueous medium due to hydroxylation

At higher pH, the equilibrium is driven towards right, as the surface tends to lose protons and become negatively charged, whereas at lower pH, the equilibrium is driven towards left and surface is positively charged. The kind of charge that gets developed at a particular pH depends on the nature of the material. For acidic oxides like silica, the charge is negative for most of the pH range, while basic oxides like MgO are positively charged at most pH values. Besides hydroxylation at the surface of the colloidal particle, a charge might also arise naturally due to several other factors driving thermodynamic equilibrium between the particle and the medium.¹ In addition to that, surfaces can also be intentionally charged by chemically attaching charged groups onto the surface, in order to enhance the colloidal stability.

At this stage, in order to understand the electrostatic interactions between the particles in a better way, it is also important to understand the concept of an electrical double layer. The charge on the surface of a colloidal particle is exactly balanced by an equal and opposite charge in the solution near the surface, resulting in the formation of an electrical double layer.¹ The first layer (called as stern layer) consists of the fixed charges close to the surface of the particle which are all of the opposite charge to that of the particle, and hence strongly attracted towards the particle. The second layer (called the diffuse layer) consists of mobile charges which are at some distance

away from the particle. The typical electrical double layer and the variation of potential as a function of distance for the case of a colloidal particle with a charged surface in a medium with dilute concentration of ions are shown in the Figure 2-2.

For two spheres of equal radius, the electrostatic interaction potential is given by

$$V_R = 32\pi\epsilon a \left(\frac{kT}{ze}\right)^2 \gamma^2 \exp(-\kappa h) \quad (2-1)$$

Where ϵ is the dielectric permittivity of the medium, k is the boltzman constant, T is the temperature, z is the ionic concentration in the medium, e is the electronic charge, γ is the function of dimensionless surface potential, κ is the Debye Huckel parameter and h is the distance between the particles.²

The characteristic parameters that describe the double layer are the zeta potential ζ and the Debye huckel parameter κ , which has the dimensions of reciprocal length, and is given by

$$\kappa^2 = \frac{2e^2 n_0 z^2}{\epsilon kT} \quad (2-2)$$

The inverse of the Debye Huckel parameter ($1/\kappa$) is a measure of the thickness of the diffuse layer and is also known as Debye length. At a distance $1/\kappa$ from the surface, the potential has fallen to a value $1/e$ of the surface potential. Thus, the Debye Huckel parameter is a measure of the extent of counterion charge in the diffuse layer. $1/\kappa$ is indicative of the range of electrical interaction between the particles. The smaller the Debye length, the smaller will be the double layer thickness and consequently, smaller will be the range of the electrostatic interaction between the particles. As we can see from the Equation 2-1, the interaction potential decays

exponentially with distance, with a decay length of $1/\kappa$. The potential due to the surface charge at the end of stern layer is called the stern potential and the potential at end of diffuse layer is called zeta potential. Thus, zeta potential is the potential difference between the dispersion medium and the edge of the diffuse layer. At constant ionic strength of the medium, higher the charge on the particle, higher will be the zeta potential. zeta potential and the Debye length are the parameters that are used to characterize the strength of electrostatic interactions between the particles.

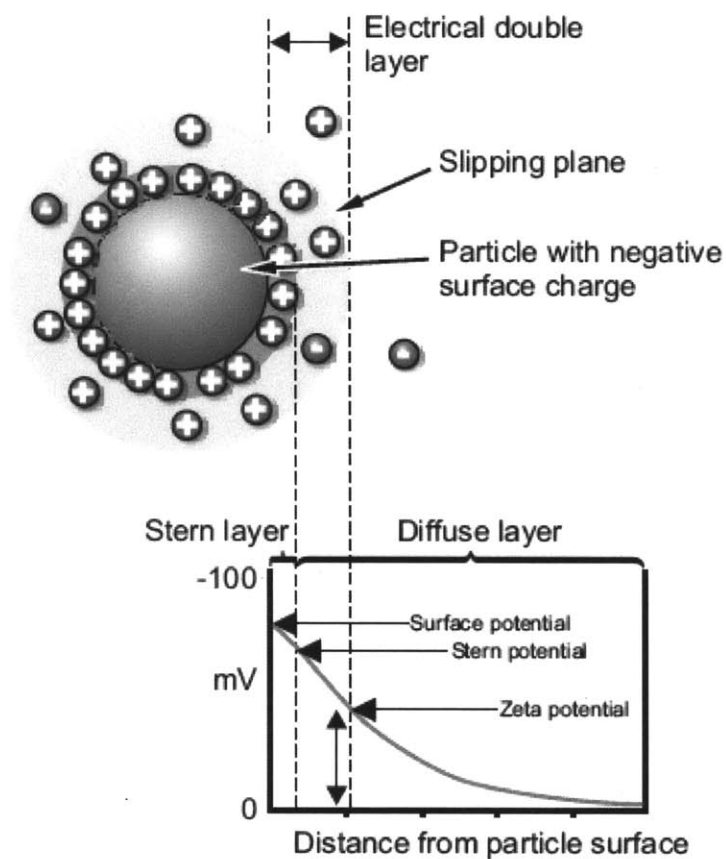


Figure 2-2: Schematic of the electrical double layer (EDL) formed across a negatively charged colloidal particle. Image Source:

<http://www.nbtc.cornell.edu/facilities/downloads/zetasizer%20chapter%202016.pdf>

Now, consider what happens when we add salt to an aqueous colloidal dispersion. In general, an increase in the ionic concentration of the system leads to a decrease in the magnitude of the zeta potential ζ and also in Debye length $1/\kappa$. Both of these lead to a decrease in the repulsion between the particles. Thus, ions in the system screen off the coulombic interactions between the particles.

Now, the medium that we are dealing with, i.e. molten salts has an extremely high concentration of ions. As a result, the Debye length becomes extremely small, and the electrostatic interactions are more or less completely screened off. It is important to note that the classical analogy (of decreasing Debye lengths and zeta potential) cannot be applied to the systems where ionic concentration is as high as in the case of molten salts, and some modifications need to be made. Firstly, in case of ionic liquids, the ions are not independent of one another, and the ion correlation effects can be quite strong. Thus, a correction factor has to be brought in when determining the effective charge concentration in the medium if Equation 2-1 is to be used. More importantly, the arrangement of charged ions close to a charged surface in molten salts is actually very different from the double layer model described above for dilute aqueous electrolyte solutions. The theory of electrical double layers has been built by placing a restriction on ion volume, and cannot be directly extended to the molten salts. In a molten salt, the screening of charges is not exactly due to oppositely charged ions in the double layer, and the potential does not decay exponentially with distance. A lot of research is currently being carried out to understand the structure and dynamics of ions at the charged surface in a molten salt medium.³ Computer simulations have indicated pronounced and long range charge density oscillations close to the interface.⁴ Figure 2-3 shows the potential across a cell consisting of charged electrodes with different surface charge densities in an ionic liquid.

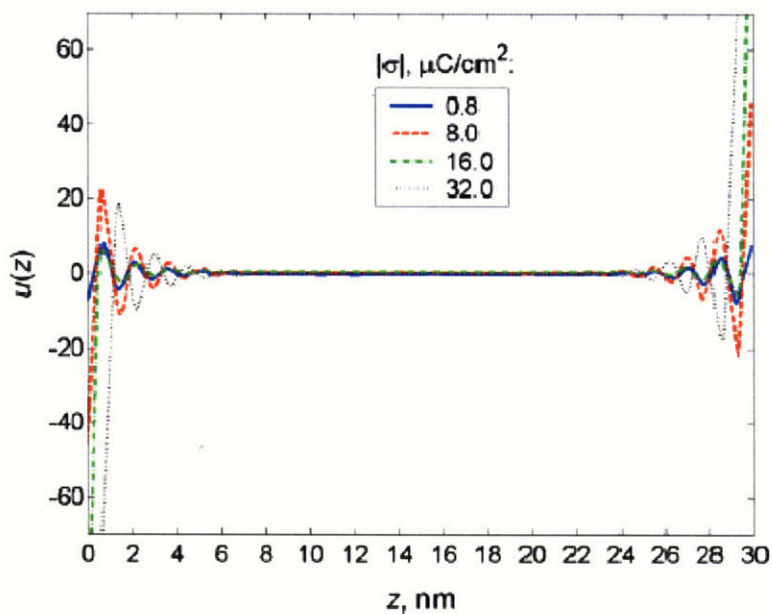


Figure 2-3: The variation of potential with distance between electrodes with different surface charge densities in an ionic liquid cell. The potential profile differs significantly from the exponentially decaying one observed in the case of an electrical double layer.⁴

The main take away from the Figure 2-3 is the fact that the charges are screened efficiently by molten salts and the effect of the charged surfaces is completely neutralized. The screening of charges takes place due to local polarization of the high density layers at the surface. One of the important results arising from the difference in screening mechanism is that molten salt responds far more quickly (~3 orders of magnitude) to changes in surface charge densities than a traditional electrolyte using double layer mechanism would.⁵ Thus, it is actually much more efficient in screening off the electrostatic interaction between charged colloidal particles. In a nutshell, even though the theory of the double layer has to be built completely differently for molten salts, the bottom line remains that the electrostatic interactions are screened off

completely by the constituent ions and charged colloidal particles are unlikely to face any repulsion when they approach one another.

2.1.2 van der Waals forces

Another very important interaction between the colloidal particles is the van der Waals force of attraction, which, in general, has three components, viz, Keesom, Debye and London forces. The Keesom force is the force of attraction between two permanent dipoles. The Debye force is the force of attraction between a permanent dipole and an induced dipole. The London force is the force that always occurs between the particles (even if there are no permanent dipoles), and is caused by spontaneous oscillations of electron clouds which generate temporary dipoles. These temporary dipoles induce temporary dipoles in neighboring atoms, and the resultant force of interaction between these two dipoles is the London dispersion force. In colloidal systems, when we talk about van der Waals forces between two colloidal particles, we essentially mean the ever-present London dispersion force. From now on, van der Waals forces and London dispersion forces will be used interchangeably in this text.

The van der Waals energy between two particles depends upon the geometry of the two particles and the Hamaker coefficient for the system. For two spherical particles of equal sizes (diameter d and distance s between the particles), the van der Waals energy of interaction is given by Equation 2-3.⁶

$$U_{Vdw} = -\frac{A}{12} H\left(\frac{s}{d}\right) \quad (2-3)$$

where,

$$H(x) = \frac{1}{2x+x^2} + \frac{1}{1+2x+x^2} + 2\ln\left(\frac{x^2+2x}{1+2x+x^2}\right) \quad (2-4)$$

The Hamaker coefficient, A , can be shown theoretically to depend upon the variation with wavelength of the complex dielectric constant of the particles and the medium. To a certain extent, it can be estimated from the refractive indices and the static dielectric constants of both particle as well as the medium.

It is not immediately intuitive that van der Waals forces of attraction depend on properties like refractive indices of the materials involved. However the intuition comes when we delve into the origin of the force. As described above, London - van der Waals forces are created by collective coordinated interactions of oscillating electric charges. They result from charge and electromagnetic field fluctuations at all possible rates. Now, frequencies at which charges spontaneously fluctuate are the same as those at which they naturally move, or resonate to absorb external electromagnetic waves. This fact helps us to understand the inherent connection between the van der Waals forces and the electromagnetic properties of the materials involved. Lifschitz developed the modern theory for estimation of the Hamaker coefficient in terms of the properties (dielectric spectrum or the absorption spectrum) of all the materials involved in the medium.⁷

Thus we see that in order to estimate the Hamaker coefficient, we need to know the material of the nanoparticles and the medium. The Hamaker coefficient between two particles of material 1, in a medium 2, is represented as A_{121} . When the Hamaker coefficient of a material is stated without specifying the medium, the medium is implied to be vacuum by default.

The data required for precise determination of Hamaker coefficients are difficult to obtain, (though possible nevertheless). Theoretically, the dielectric response over the entire frequency range from zero to infinity is required. However, for all practical purposes, accurate estimation of the Hamaker coefficients using the full spectral formulation of Lifschitz can be made if

relevant dielectric data are available for 0 to 40 eV. As even this information is rarely available, most estimation of Hamaker coefficients are based on approximations, which use just the visible refractive index of the materials involved, instead of the entire spectrum over all the wavelengths. Equation 2-5, known as the Tabor Winterton Approximation (TWA) gives the approximate value of the Hamaker coefficient.⁸

$$A_{121}^{TWA} = \frac{3\pi\hbar V\epsilon}{8\sqrt{2}} \frac{(n_{vis0,1}^2 - n_{vis0,2}^2)^2}{(n_{vis0,1}^2 + n_{vis0,2}^2)^{\frac{3}{2}}} \quad (2-5)$$

Where,

A_{121}^{TWA} = The Hamaker constant for 'material 1' with 'material 2' as the medium,

$n_{vis0,1}^2$ = Visible refractive index of 'material 1' in vacuum

$n_{vis0,2}^2$ = Visible refractive index of 'material 2' in vacuum

ν_e = plasma frequency $\sim 3 \cdot 10^{15}$ Hz for ionic liquids

\hbar = Planck's constant

Another important empirical approximation is widely used for estimation of the Hamaker coefficient of particles of material "1" in medium "2", if the Hamaker coefficient in vacuum is known for materials of both the particles and the medium.

The Hamaker coefficient of the particles "1" interacting across the medium "2" is given by

$$A_{121} = \left(A_{11}^{\frac{1}{2}} - A_{22}^{\frac{1}{2}} \right)^2 \quad (2-6)$$

An important point to note is that the Hamaker coefficient itself depends on the distance between the particles. If the particle distance increases, the coordinated motion of the charges

between the two interacting particles falls out of sync which leads to reduction of the Hamaker coefficient. This effect is known as retardation. When the interacting particles are in contact, we have the non retarded Hamaker coefficient, which is constant for the given particles and the medium and hence also known as the Hamaker constant. Henceforth in this document, unless otherwise mentioned, the term Hamaker coefficient will mean the non-retarded Hamaker coefficient. We will discuss the full spectral Lifschitz formulation for obtaining the Hamaker coefficients in Chapter 4.

It must be noted that in principle, the interaction energy (and force of attraction) due to London van der Waals forces will become infinite at contact, as suggested by 2-3. This, as we know is obviously not the case. If it was, it would be impossible to break clusters of particles by stirring or sonication. At very close approach, short range repulsion forces like Born repulsion come into the picture, and prevent the separation distance from becoming absolutely zero. The equilibrium separation distance between the particles apparently in contact is normally between 0.1-0.2 nm.⁹ This finite distance ensures that the van der Waals force too remains finite. Furthermore, the roughness of the surface will also play an important role in limiting the minimum separation distance between the particles. We will revisit this particular concept and evaluate the possibility of using this to our advantage in chapter 4.

2.2 DLVO theory of colloidal stability

In section 2.1 we considered in some detail two of the most important forces of interaction between colloidal particles, which are largely responsible for determining the colloidal stability. These forces form the basis of the DLVO theory of colloidal stability, developed by Derjaguin and Landau (1941)¹⁰ and Verwey and Overbeek (1948).¹¹

DLVO theory is a well established framework that considers total interaction energy between any two particles as a function of particle separation and helps to predict whether or not a particular suspension will be colloidally stable. Essentially, the total energy of interaction between the particles is simply given by the addition of the van der Waals attraction and the electrical double layer repulsion. Thus,

$$U_T = U_{vdW} + U_{EDL} \quad (2-7)$$

The variation of interaction energy with distance between the particles can take several different forms, depending upon the relative strengths of various parameters such as particle size, zeta potential, Debye length and Hamaker coefficient that determine the van der Waals and electrical double layer interactions. The typical shape of the DLVO curve for most colloidal systems is presented in Figure 2-4 below. As shown, the vdW force of attraction and EDL force of repulsion together result in one maximum (called the primary maximum), and two minima (primary and secondary minima). The shape of the "net" DLVO potential determines the colloidal stability and the aggregation rate of the particles. The primary maximum represents an energy barrier that needs to be crossed if the two approaching particles are to come in contact and agglomerate. The higher the barrier, the lower will be the aggregation rate, as more particle-particle approaches will be repelled due to the barrier. In a colloidal system, the kinetic energy that approaching particles have is due to the Brownian motion. The energies of the particles follow a Gaussian distribution with kT as the mean. If the particles are charged, the strong electrostatic repulsion force between the particles will ensure a large energy barrier, which would lead to a colloidally stable system.

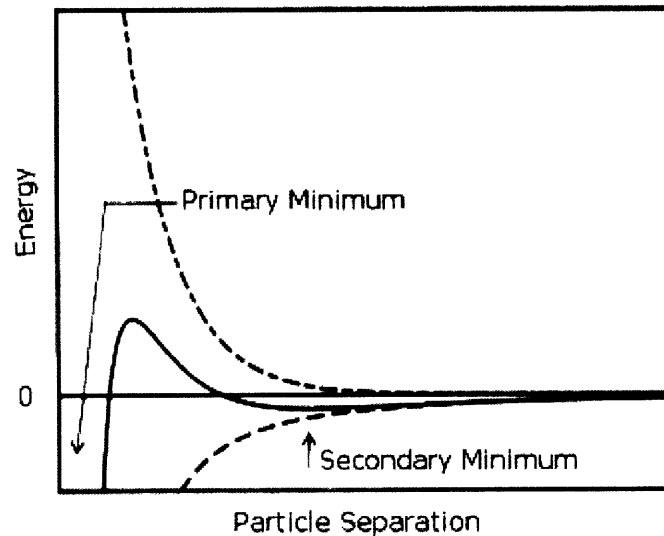


Figure 2-4: A typical DLVO potential curve. It is the summation of the electrostatic and van der Waals interaction energy, which results in a one maximum and two minima.

Again, it is important to note that in principle, the van der Waals force will be infinitely strong at contact and the primary minimum will be infinitely deep. This will mean that no two particles which come in contact could ever be separated. However, the short range Born repulsion forces, hydration effects and surface roughness all combine to ensure that the attraction force (and hence the depth of primary minimum) remains finite. So if a breaking energy greater than the depth of the primary minimum is provided to a two-particle aggregate, the aggregate would disintegrate into its individual constituent particles. The secondary minimum brings in a few more nuances in the aggregation process in some colloidal systems, and can be responsible for weak large range aggregates. For now, we will neglect the effects of the secondary minimum because it does not play any significant role in the system of our interest.

The parameter that determines the colloidal stability is the collision efficiency (or sticking coefficient) α , which is the fraction of particle collisions that lead to sticking. As should be obvious by now, the value of α depends on the DLVO profile. The reciprocal of α is called the

stability ratio W , which is the ratio of aggregation rate in absence of colloidal interactions to that found when there is repulsion between the particles. For a purely DLVO system (neglecting hydration effects, which will be discussed later), an expression was derived for the stability ratio by Fuchs by treating the problem as that of diffusion in a force field.¹² The expression for W is given in Equation 2-8.

$$W = 2 \int_0^{\infty} \frac{\exp(\Phi_T/kT)}{(u+2)^2} du \quad (2-8)$$

where Φ_T is the total interaction at a particle separation distance d . u is a function of d and particle size. For spherical particles of different radii a_i and a_j , u is given by

$$u = \frac{2d}{a_i + a_j} \quad (2-9)$$

For equal sized particles this just becomes $u=d/a$. Reerink and Overbeek made an approximation by making use of the fact that the region close to the maximum contributes a large portion of the integral.¹³ Equation 2-8 then gets reduced to

$$W = \frac{1}{\kappa(a_i + a_j)} \exp(\Phi_{max}/kT) \quad (2-10)$$

In Equation 2-10, the stability ratio just becomes a function of the Debye length and the barrier height, rather than the entire DLVO profile. From Equation 2-10, we find that for ionic concentration of 0.1M and particle size of 1 μ m, if the barrier height is 20 kT, roughly one in a million approaches will have the energy to cross the barrier. Equation 2-10 helps us to easily

connect between the barrier height and the collision efficiency. So far we have been talking about the general colloidal system. However, as we saw earlier, the system of interest is quite unique because of the fact that all the electrostatic charges are completely screened. So, the DLVO potential profile of particles in molten salt medium will not exhibit an energy barrier. We can see the effect of increasing salt concentration on the height of the DLVO primary maximum in Figure 2-5.¹⁴ It shows how the DLVO potential of gold nanoparticles dispersed in water is affected by increasing salt concentration in water. As the concentration increases, the EDL interactions between the particles decrease and consequently, the DLVO energy barrier decreases. As can be seen, at 1M NaCl concentration there is hardly any energy barrier to prevent the agglomeration of gold particles. When the value of the primary maximum becomes zero, i.e. when the energy barrier disappears completely, the sticking coefficient ideally will become equal to 1.

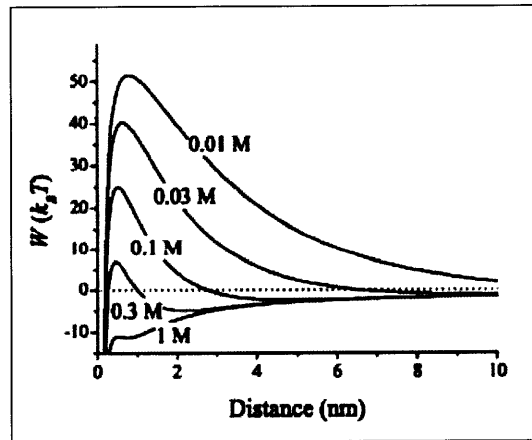


Figure 2-5: Variation of DLVO energy barrier with increasing salt concentration. As the salt concentration increases, the energy barrier decreases due to the screening of electrostatic interactions¹⁴

The number of ions in a molten salt will be much higher than those in 1M salt solution. In fact, as we saw earlier, molten salts are much more efficient in screening the charges than an aqueous electrolyte of similar ionic conductivity. Hence it is reasonable to expect that the DLVO energy barrier will completely disappear when the medium of dispersion is a molten salt, as is indeed the case. Figure 2-6 compares the DLVO energy barrier for charged silica particles in 0.1 M 1:1 salt aqueous solution and that in different ionic liquids. As can be seen, the DLVO energy barrier disappears when charged silica is dispersed in an ionic liquid.¹⁵

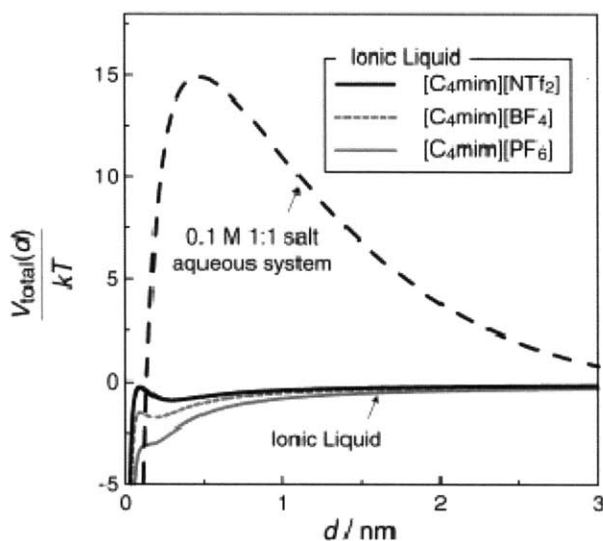


Figure 2-6: Effect of charge screening by ionic liquids on the energy barrier¹⁵

The variation of stability ratio with increasing ionic concentration in a medium is of interest. As shown in Figures 2-5 and 2-6, the DLVO energy barrier decreases with increasing salt concentration in an aqueous system. This will lead to a decreasing stability ratio and increasing sticking coefficient. Figure 2-7 presents a schematic diagram showing the effect of increasing salt concentration on stability ratio.¹ On a log-log plot, the variation of the stability ratio with the

salt concentration is linear. However, the stability ratio does not decrease indefinitely as the salt concentration is increased. When the salt concentration is high enough to suppress the potential barrier completely, further increases in salt concentration do not lead to any significant change in stability ratio. This concentration at which the barrier disappears is known as critical coagulation concentration (CCC). After this concentration, the stability ratio becomes equal to 1 and all collisions lead to aggregation.

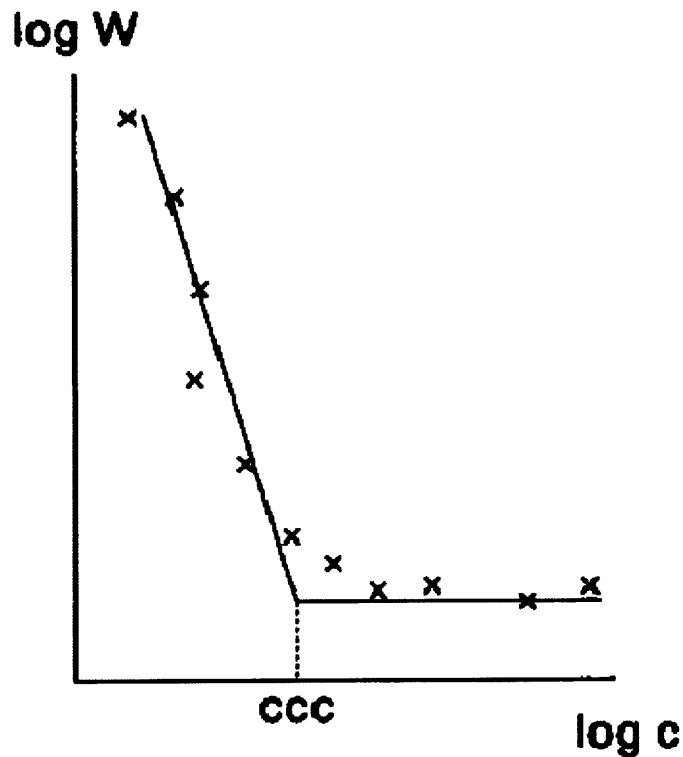


Figure 2-7: Variation of stability ratio with salt concentration. The stability ratio initially decreases linearly with increasing salt concentration, and becomes constant after reaching the critical concentration.¹

The fact that the stability ratio does not decrease beyond the CCC has an important consequence for our system consisting of a molten salt medium. CCC represents the point where the primary maximum becomes zero. Even beyond the CCC, increasing salt concentration will still keep lowering the primary maximum into the negative, as we can see in Figure 2-5. In other words, attraction between the particles will keep increasing with increasing salt concentration after the CCC, until the net DLVO curve coincides completely with the van der Waals attraction curve. However, this attraction between the particles is rarely sufficiently long range to have any significant impact on the collision frequency. That is to say, the collision frequency is largely dominated by the Brownian motion, and hence depends mainly on the diffusion coefficient of the particles. The rate of aggregation is simply the rate of collisions times the collision efficiency (or sticking coefficient). Brownian motion determines the collision rate, and the DLVO forces determine the sticking probability. Thus, we can say that aggregation rate will only depend upon the colloidal interaction when there is repulsion between the particles. In that case, not all collisions will lead to aggregation, and the collision efficiency will depend upon the Hamaker coefficient, Debye length and zeta potential. But once there is no repulsion between the particles, the aggregation rate depends very little on how strong the van der Waals interaction is between the particles. In the case of molten salt, the EDL interaction between the colloidal particles will be completely suppressed due to total screening of charges. Thus, if we only consider the effect of DLVO forces and neglect the hydration and viscous effects, the Hamaker coefficient is expected to have very little effect on the aggregation rate of nanoparticles.

2.3 Non DLVO forces: Hydrodynamic effects

The DLVO theory does not take into account effect of viscosity of the medium. These effects can sometimes play a significant role in determining the aggregation kinetics. Due to the no slip condition at the boundary, the liquid between the particles does not drain out easily which slows the aggregation process. In other words, the diffusion coefficient is reduced as particles approach each other due to the hydrodynamic interaction between the particles. No slip condition at the interface makes the diffusion coefficient approach zero as the particles come into contact. Ideally, in such a case, the particles would never aggregate. However, the van der Waals attraction between the particles brings them together by negating the viscous resistance at close approach. Quite clearly, van der Waals forces become more important in determining the aggregation rate when we do take into account the hydrodynamic interactions between the particles. Honig ¹⁶ reported an empirical approximation for the variation of the diffusion coefficient with particle separation for an aqueous suspension.

$$\frac{D(u)}{D(\infty)} = \frac{6u^2+4u}{6u^2+13u+2} = \frac{1}{\beta(u)} \quad (2-11)$$

Here,

u - dimensionless distance $u=d/a$

$D(u)$ – diffusion coefficients for particles separated by distance u

$D(\infty)$ – diffusion coefficients for particles at infinite separation

$\beta(u)$ is a correction factor that needs to be applied between every pair of particles. Physically, it means that the diffusion coefficient is reduced at a separation u by this correction factor. The

impact of viscous effects can be fairly long range. Equation 2-11 has been developed for water. The extent of hindrance these hydrodynamic effects provide depends not only on the physical properties such as the viscosity of the medium, but also on the nature of bonding close to the particle surface. Adhesive water layers form close to the surface of the particles due to hydrogen bonding between water molecules. The description of $\beta(u)$, hence will be different for different media. The example of water, can however be used as a general reference for qualitative arguments.

If we correct for the hydrodynamic interactions in the equation for stability ratio, we get:

$$W_{lim} = 2 \int_0^{\infty} \beta(u) \frac{\exp(\Phi_T/kT)}{(u+2)^2} du \quad (2-12)$$

In the case of an electrically fully destabilized system (like particles in molten salts), Φ_T will just be the van der Waals interaction energy. One can now obtain the variation of stability ratio with Hamaker coefficient for the case of water, with and without taking into consideration the hydrodynamic interaction.

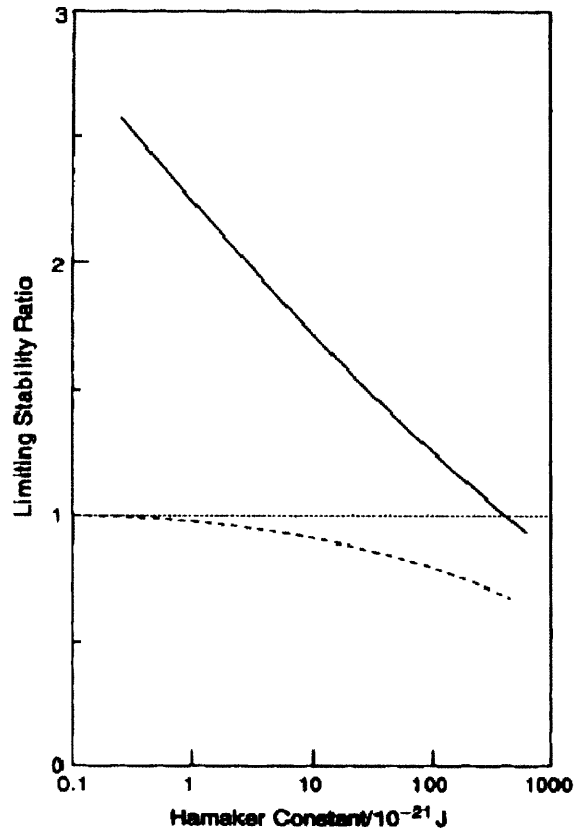


Figure 2-8: Variation of limiting stability ratio versus the Hamaker coefficient taking into consideration the hydrodynamic interactions (Solid line). The dotted line shows the variation when hydrodynamic interactions are not considered.¹

As we see in Figure 2-8, the limiting stability ratio varies significantly with Hamaker coefficient when the hydrodynamic effects are taken into consideration. The stability ratio for particles with Hamaker constant 1 zJ is approximately twice that at 100 zJ. Most colloidal materials will fall within this range of Hamaker constant. Also, as discussed before, when only DLVO forces are considered, the variation is little and unlikely to result in any significant change in aggregation rate.

2.4 Smoluchowski model of aggregation kinetics

Having considered the nature of different interactions in a colloidal system, we turn our attention to the models for aggregation rates. Smoluchowski first developed a model for the aggregation process in 1917.¹⁷ It is regarded as a classic work in the field and is still the starting point of most discussions on aggregation. The model is based on the assumption that the rate of collision between two sizes of particles is proportional to the concentration of the particles with those sizes. So, if there are n_i particles of size i and n_j particles of size j , then the number of collisions occurring between them in a unit time and unit volume will be given by Equation 2-13.

$$J_{ij} = k_{ij}n_in_j \quad (2-13)$$

Here k_{ij} depends on various factors like particle size, fluid properties, and the dominant mechanism of aggregation. Also, it is important to note that in this model, aggregation is assumed to be a second order process, and three (or more) body collisions are ignored.

When all collisions produce aggregates, as is likely in the case of molten salts, the aggregation rate is the same as the collision rate. When there is a repulsive interaction between the particles, or when the hydrodynamic hindrance is significant, we need to take into account the collision efficiency α , which is just the inverse of the stability ratio. In this case, the rate of aggregation is

$$J_{ij} = \alpha k_{ij}n_in_j \quad (2-14)$$

In the smoluchowski model, the particles are assumed to coalesce and form a bigger spherical particle with a volume equal to the total volume two colliding particle. While this assumption is

not strictly valid except in the case of liquid droplets, it is still found to yield reasonable estimates of aggregation kinetics of particles in an isotropic field.

Now, the effective rate of creation of k sized particles can be written as:

$$\frac{dn_k}{dt} = \frac{1}{2} \sum_{i=1, i+j \rightarrow k}^{i=k-1} k_{ij} n_i n_j - n_k \sum_{k=1}^{\infty} k_{ik} n_i \quad (2-15)$$

The first term represents creation of k sized particles from two smaller sized particles of sizes i and j. The second term represents destruction of a k sized particle due to its agglomeration with another particle to form a bigger particle.

While Equation 2-15 has been derived with discrete particle sizes in mind, an equivalent form for continuous particle size distribution has been established by G. M. Hidy.¹⁸ The integral form is shown in Equation 2-16.

$$\frac{\partial n(i,t)}{\partial t} = \frac{1}{2} \int_0^i k(i-j, j) n(j, t) n(i-j, t) dj - n(i, t) \int_0^{\infty} k(i, j) n(j, t) dj \quad (2-16)$$

2.4.1 Mechanisms of collisions

The main parameter that needs to be evaluated in order to make use of Equations 2-15 and 2-16 is the collision rate k_{ij} , which depends upon the dominant mechanism of collision. The process of aggregation can take place through three main dominant mechanisms, viz. perikinetic

aggregation, orthokinetic aggregation and differential settling. The value of collision constant k depends upon the mechanism of collision.

2.4.1.1 Perikientic Aggregation

Perikinetic aggregation is dominated by Brownian motion and the resultant collisions between the particles. This is the dominant mechanism for nanoparticles in stationary fluid, as the force of gravity is negligible in comparison to Brownian force. The rate constants for perikinetic collisions is given by Equation 2-17.¹

$$k_{ij} = \frac{2kT}{3\mu} \frac{(a_i + a_j)^2}{a_i a_j} \quad (2-17)$$

Where

kT – Thermal energy

μ – viscosity

a_i, a_j – sizes of the colloid particles

For equal sized particles, the expression reduces to

$$k_{ij} = \frac{8kT}{3\mu} \quad (2-18)$$

2.4.1.2 Orthokinetic aggregation

Orthokinetic aggregation occurs due to collisions of particles brought about by motion of the fluid (due to flow, stirring etc.) which can lead to enormous increase in the rate of interparticle collisions. In our case, we will be mainly dealing with a stationary molten salt, so the

orthokinetic component will come only from any convective currents that exist in the system. In such a case, without any apparent flow of the fluid medium, the contribution of orthokinetic aggregation is expected to be insignificant compared to perikinetic aggregation. Also, shear forces acting on aggregates can also lead to breaking of aggregates, which needs to be taken into account when dealing with Orthokinetic aggregation. The collision rate constant in this mode of transport is given by Equation 2-19¹.

$$k_{ij} = \frac{4}{3} G \frac{(a_i + a_j)^2}{a_i a_j} \quad (2-19)$$

2.4.1.3 Differential settling

The third important collision mechanism is when larger particles settling under gravity collide with slower settling smaller particles on their way. This normally becomes the dominant mechanism of collision when particle sizes are large enough to be affected by gravity (typically of the order of 10 μ). The collision rate constant when differential settling is dominant is given by Equation 2-20¹.

$$k_{ij} = \left(\frac{2\pi g}{9\mu} \right) (\rho_s - \rho) (a_i + a_j)^3 (a_i - a_j) \quad (2-20)$$

For our problem, when nanoparticles are dispersed in a molten salt, we expect that the particles would initially aggregate due to Brownian collisions whereas later, when larger clusters are formed, differential settling collisions will be the primary mechanism.

2.5 Studies of colloidal stability in Ionic liquids

There are factors beyond DLVO forces that can play a very important role in determining the aggregation rate of colloidal particles in various systems. Hydration and solvation forces can depend greatly upon the interface characteristics of the system. The closest system comparable to molten salts that have been studied in some detail in the literature are ionic liquids. Ionic liquids are, in principle molten salts, but they liquefy at room temperature. However, the ions which are present in these room temperature liquefying salts are of a different kind. They mostly contain at least one organic ion, which is significantly greater in size as compared to inorganic ions such as alkali ions, halides, or even nitrates. While the basic fundamental properties like charge screening remain pretty much the same in ionic liquids and molten salts, there can be several effects due to the large size of the ions which could alter the aggregation behavior of colloidal particles in the two media. If we just go by the DLVO forces, all bare nanoparticles will agglomerate rapidly in ionic liquids, as there will not be any repulsion between the particles. Thus any attempts of electrostatic charge stabilization are likely to fail. However, some transition metal nanoparticles like gold show very good colloidal stability in ionic liquids even in the absence of stabilizers or polymers.¹⁹ Even silica nanoparticles have been found to show greater colloidal stability than expected in a completely destabilized system.²⁰ Detailed understanding of stabilization or aggregation of nanoparticles in ionic liquids has not yet been achieved, and it is an active area of research. However, one of the important factors is steric hinderance derived from adsorption of the bulky ions of the ionic liquid. These ions are large enough to separate colloidal particles by forming protective layers in the presence of strong binding interaction between the ionic liquids and the colloidal surface. Another phenomenon that is believed to affect colloidal stability is formation of a structured hydration layer at the particle surfaces by

ionic liquids due to hydrogen bonding, cation- π , and van der Waals interactions between the ions. Most of the currently understood stabilizing mechanisms are based on typical properties that bulky organic ions contribute, and such colloidal stabilization is unlikely to exist in the case of inorganic molten salts. Even if there is strong bonding between the ions and the colloidal particle, the size of an inorganic ion is far smaller than that required to provide significant steric hindrance.

Thus, in a nutshell, our system is an uncomplicated colloidal system. There is no energy barrier. There are no secondary minima effects. In principle, all the collisions will lead to sticking and aggregation, i.e. the stability ratio and collision efficiency are both equal to 1, but for the viscous effects. Thus, in a way it becomes one of the simplest colloidal systems scientifically. However, it makes our task of trying to make a colloidally stable dispersion in molten salts extremely difficult. A small preliminary experiment was done to demonstrate the effect that charge screening has on the stability of the particles, which will effectively summarize the entire theory that we discussed in this chapter. A small amount (10mg) of titania nanopowder with a size <25 nm was dispersed in at the same time in 20 ml of distilled water and 20 ml of water saturated with NaCl. Both suspensions were sonicated for 30 minutes and were then left undisturbed and allowed to settle. As we can see in Figure 2-9, the suspension in the salt solution settled much faster than that in water. This clearly demonstrates the kind of problem we are up against.

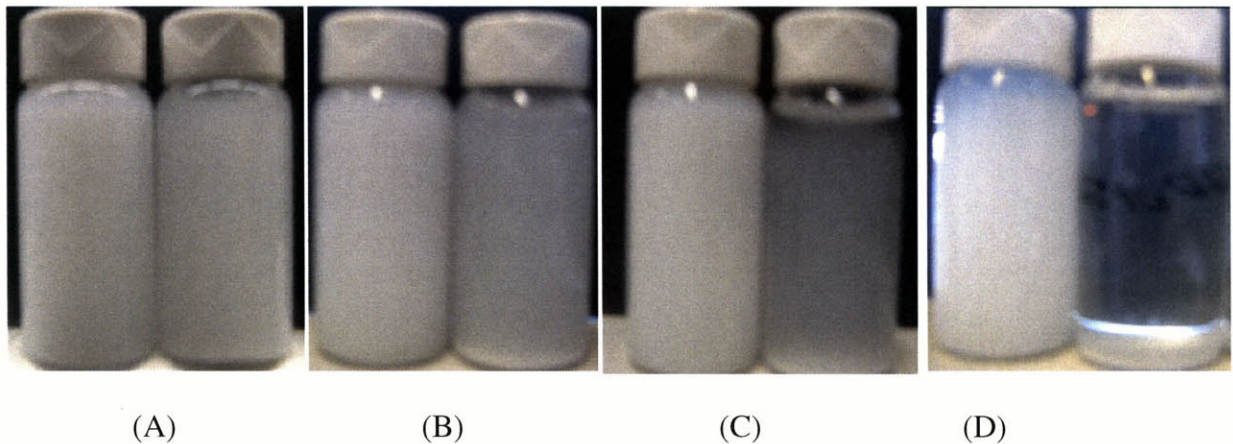


Figure 2-9: Comparison of settling rates of titania nanoparticles in pure water and water saturated with NaCl. The vial on the left is the one with pure water. The snapshots were taken instantaneously after sonication (A), after 20 minutes (B), after 120 minutes (C) and after 8 hours (D). The nanoparticles aggregate and settle in the salt solution at a much higher rate

In order to provide colloidal stability to an otherwise electrically destabilized system like this one, long polymeric surfactants are attached onto the surface of the colloidal particles, as shown in Figure 2-91 (A). The surfactant essentially provides steric hindrance and restricts the close approach of the particles. Thus, it keeps them at a distance where the thermal energy of the particles will be sufficient to counter the attraction force (if any), thereby keeping the particles suspended. This is a very standard technique used to successfully stabilize nanofluids in all kinds of medium. Even in ionic liquids, silica particles have been dispersed successfully and colloidally stabilized by polymer grafting onto their surfaces.²¹ However, here comes another constraint of our system into picture, which is the extreme temperature. None of the organic polymers will survive the high temperatures that we are dealing with (300-1000 °C) and hence steric stability using organic polymers cannot be provided to colloidal particles in molten salts.

Thus, the problem of making a colloidally stable suspension of nanoparticles in molten salts is an extremely challenging one, since none of the traditional methods of providing colloidal stability to nanoparticles (electrostatic and steric stabilization) will be effective for this system. In this thesis, we will look into the possibility of imparting long term colloidal stability to nanoparticles by reducing the van der Waals forces of attraction between them. Before that, we will experimentally observe the colloidal behavior of some nanoparticles in molten salts, and study the dependence of aggregation kinetics on various parameters such as the particle size, initial concentration of nanoparticles and temperature.

2.6 References

1. Williams, R. A., Particle Deposition and Aggregation: Measurement, Modelling and Simulation. Butterworth Heinemann: 1995.
2. Buff, F. P.; Stilling, F. H., Statistical Mechanical Theory Of Double-Layer Structure And Properties. Journal Of Chemical Physics 1963, 39, (8), 1911-&.
3. Kornyshev, A. A., Double-layer in ionic liquids: Paradigm change? Journal Of Physical Chemistry B 2007, 111, (20), 5545-5557.
4. Fedorov, M. V.; Kornyshev, A. A., Towards understanding the structure and capacitance of electrical double layer in ionic liquids. Electrochimica Acta 2008, 53, (23), 6835-6840.
5. Lanning, O. J.; Madden, P. A., Screening at a charged surface by a molten salt. Journal Of Physical Chemistry B 2004, 108, (30), 11069-11072.
6. Hamaker, H. C., The London - Van Der Waals attraction between spherical particles. Physica 1937, 4, 1058-1072.
7. Lifshitz, E. M., The Theory Of Molecular Attractive Forces Between Solids. Soviet Physics JETP-USSR 1956, 2, (1), 73-83.
8. Tabor, D.; Winterton, R. H., Direct Measurement Of Normal And Retarded Van Der Waals Forces. Proceedings Of The Royal Society Of London Series A-Mathematical And Physical Sciences 1969, 312, (1511), 435-&.
9. Israelachvili, J., Intermolecular and surface forces. 2nd ed.; Academic press: London, 1992.
10. Derjaguin, B.; Landau, L., Theory Of The Stability Of Strongly Charged Lyophobic Sols And Of The Adhesion Of Strongly Charged-Particles In Solutions Of Electrolytes. Progress In Surface Science 1993, 43, (1-4), 30-59.
11. Verwey, E.; Overbeek, J., Theory of stability of lyophobic colloids. Dover publications: 1948.
12. Fuchs, N., Ueber Die Stabilität und Aufladung der Aerosole. Z. Physik 1934, 89, 736-743.
13. Reerink, H.; Overbeek, J. T. G., The Rate Of Coagulation As A Measure Of The Stability Of Silver Iodide Sols. Discussions Of The Faraday Society 1954, (18), 74-84.
14. Butt, H. J.; Graf, K.; Kappl, M., Physics and Chemistry of Interfaces. Wiley Interscience: 2003.
15. Ueno, K.; Watanabe, M., Ionic liquids: from knowledge to applications, Chapter 14: silica colloidal suspensions in ionic liquids. American chemical society: 2009; Vol. 1030, p 199-210.
16. Honig, E. P.; Roeberse, G. J.; Wiersema, P. H., Effect Of Hydrodynamic Interaction On Coagulation Rate Of Hydrophobic Colloids. Journal Of Colloid And Interface Science 1971, 36, (1), 97-&.
17. Smoluchowski, M., Versuch einer mathematischen Theorie der Koagulationskinetik Kolloidaler Lösungen. Z. Phys. Chem. 1917, 92, 129-168.
18. Hidy, G. M., On Theory Of Coagulation Of Noninteracting Particles In Brownian Motion. Journal Of Colloid Science 1965, 20, (2), 123-&.
19. Schrekker, H. S.; Gelesky, M. A.; Stracke, M. P.; Schrekker, C. M. L.; Machado, G.; Teixeira, S. R.; Rubim, J. C.; Dupont, J., Disclosure of the imidazolium cation coordination and stabilization mode in ionic liquid stabilized gold(0) nanoparticles. Journal Of Colloid And Interface Science 2007, 316, 189-195.
20. Ueno, K.; Imaizumi, S.; Hata, K.; Watanabe, M., Colloidal Interaction in Ionic Liquids: Effects of Ionic Structures and Surface Chemistry on Rheology of silica Colloidal Dispersions. Langmuir 2009, 25, (2), 825-831.

21. Ueno, K.; Inaba, A.; Kondoh, M.; Watanabe, M., Colloidal stability of bare and polymer-grafted silica nanoparticles in ionic liquids. *Langmuir* 2008, 24, (10), 5253-5259.

3. Estimation of aggregation kinetics in molten salts by turbidity measurements: Experimental results

3.1. The objective and methodology of experiments

Our task is to study the aggregation and sedimentation kinetics of nanoparticles in molten salts. As we saw in the last chapter, many factors can affect the colloidal stability of particles in a particular medium. Detailed understanding of interparticle interactions, of fluid properties and of the dynamics at the particle-medium interface is required in order to accurately predict the behavior of a colloidal system. To the best of our knowledge, the problem of colloidal stability in high temperature inorganic molten salts has not been explored at all in the literature. As discussed in chapter 2, the molten salt medium could generically be compared to saturated aqueous salt solution or ionic liquids, in the sense that the coulombic interactions between the particles are completely screened and the DLVO collision efficiency is expected to be equal to 1. However, non DLVO interactions like hydrodynamic interactions exist in colloidal systems which make each system unique and no direct correspondence can be drawn between molten salts and either of the other two mediums stated above. We can, however, expect the colloidal stability of nanoparticles in the molten salts to be really poor.

It is important to note that we are interested not only in aggregation of particles but also their sedimentation. The process can be considered a two step process, where the particles first aggregate due to collisions during random Brownian motion, and then sediment after having achieved a certain aggregate size. Obviously, both these processes occur simultaneously. As far as applications are concerned, sedimentation time is one of the important parameters that we

would be interested in, as it would determine the time interval in which the salt needs to be agitated. Hence, it is important to determine experimentally the settling rates of nanoparticles in molten salts, and observe their variation with different salts, different particles, different concentrations and different temperatures.

3.1.1 Selection of salts and nanoparticles

Short listing the possible particles that can be used to form dispersions in molten salts begins with the most important of the requirements, which is physical and chemical stability at temperatures as high as 1000 °C. This immediately eliminates almost everything apart from high temperature metal oxide ceramics with melting point greater than 1500 °C. A few appropriate materials that we would consider for this study are SiO₂, TiO₂, Al₂O₃ etc.

As discussed before, there are two main categories of molten salts that we are interested in, viz, the chloride salts and the nitrate salts. The main difference between the two is the temperature of melting. While alkali nitrate salts melt at lower temperatures (250 °C-350 °C), and are stable only up to ~550 °C, pure alkali chloride salts melt at a much higher temperatures (800 °C). We have taken Sodium nitrate (M.P. 308 °C) as representative of nitrate salts and a 50-50 (wt%) mixture of sodium chloride (NaCl) and potassium chloride (KCl) (M.P. 658 °C) as representative of chloride salts. The main properties of the medium and particles that may affect the aggregation kinetics of particles are their refractive indices (different van der Waals interaction), density (different sedimentation rate), viscosity of the medium (different collision rate and sedimentation), etc. Note that all of these properties vary with temperature, and hence temperature is expected to play a significant role in the aggregation and sedimentation rate.

3.1.2 Method of dispersing nanoparticles in molten salts

The salts were melted in a furnace consisting of two 120V semi-cylindrical heaters purchased from Watlow, measuring 3.5” in diameter and 6” in height. A probe sonicator purchased from Sonic inc was used for dispersion of particles in the molten salt. The set up is shown in Figure 3-1. For nitrate salts, the nanoparticles were initially dispersed in acetone by adding the measured quantity of commercial nanopowder to acetone and sonicating the suspension for 30 minutes. The resulting nanofluid in acetone was then injected into the bulk of the molten salt using a syringe and a needle. Acetone vaporized out of the system very quickly (~ 30 seconds) leaving the nanoparticles behind in the molten salt. This was followed by sonication of the nanoparticles laden molten salts for about 5 minutes using the probe sonicator. Practically, the process of injecting acetone into the salt was not much different than dropping acetone droplets onto the surface of the salt, because the large difference in density between acetone and the molten salt ensured that acetone droplets would quickly come to the surface anyway. However, to maintain consistency throughout the sets of experiments, the injection method was followed. For chloride salts, use of an organic solvent like acetone was deemed inappropriate because any organic solvent would flash at the melting point of chloride salts. For example, the flash point of acetone is 456°C, while the melting point of 50/50 NaCl/KCl is 658 °C. Hence, in chloride salts, particles were dispersed by directly sonicating the nanopowder containing molten salt. With nitrate salts, it was observed that settling behavior of particles was similar with both the methods of initial dispersion, and hence direct sonication of molten chlorides with nanopowder was deemed acceptable.

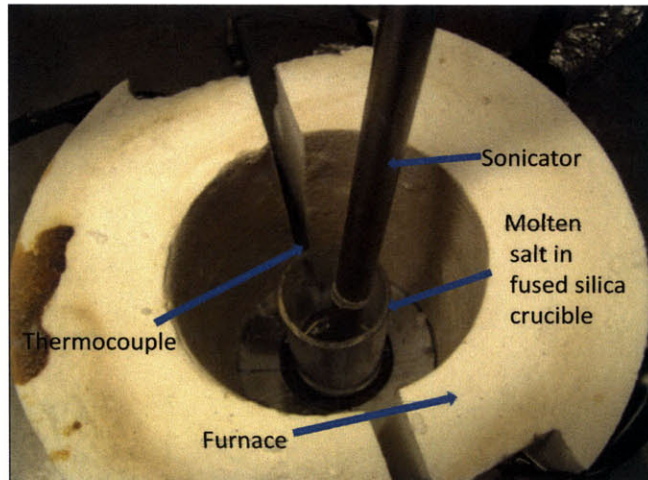


Figure 3-1: Experimental set up for dispersing the nanoparticles in molten salts.

Sonication of molten salts using a probe sonicator has its own share of issues. The length of the sonication probe is tuned so that its natural frequency of vibration matches that of the piezoelectric crystal of the sonicator. The allowance for this length is very small ($<0.1\%$). At high temperatures, as the probe expands, the natural frequency of vibration of the probe falls out of sync with the vibrating frequency of the sonicator, which causes the sonicator to shut down. The higher the temperature, the sooner the shutdown occurs. In our case, the sonicator could sonicate for around two minutes in nitrate salts ($350\text{ }^{\circ}\text{C} - 450\text{ }^{\circ}\text{C}$), and around 30 seconds in chloride salts. Once shut down, the sonicator probe had to be quenched in water and the sonicator had to be restarted before the sonication process could continue. Consequently, the sonication of nanopowder in molten salt was more of an intermittent process, rather than a continuous one.

3.1.4 Estimation of settling rates

After the particles were dispersed, the settling behavior of the nanoparticles was monitored as a function of time. Periodic photographs of the suspension were taken to observe the variation in turbidity of the suspension as it settled over time. In order to quantify the turbidity, attenuation of the intensity of a laser beam passing through the suspension was measured at different time intervals. A laser pointer was used as a laser source, and a SpectraWiz spectrometer was used to measure the intensity of the received light. This apparatus is shown in Figure 3-2.

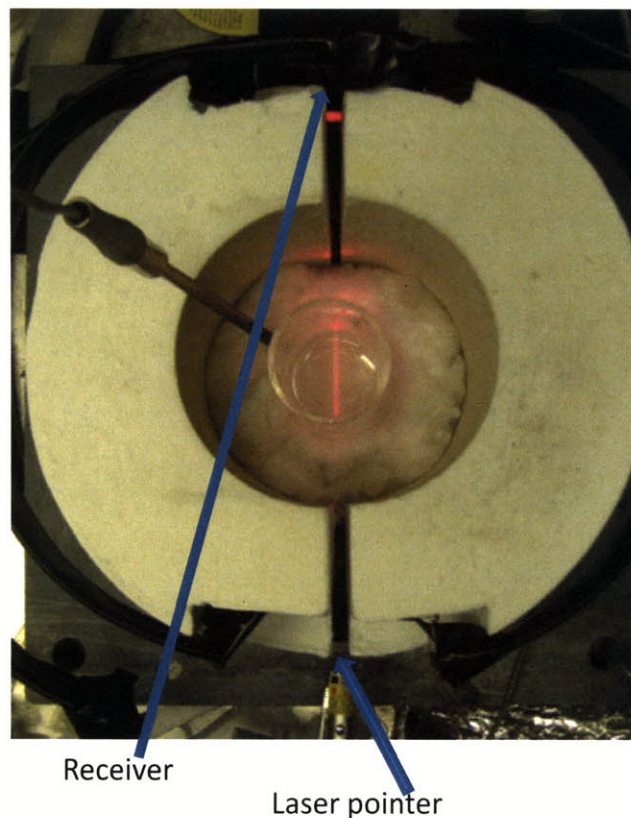


Figure 3-2: Experimental set up used to measure turbidity of suspensions over a period of time. A Laser pointer was used as the light source and a spectrometer was used to measure the intensity of received light. Measurements were taken at periodic intervals of time.

Turbidity (attenuation coefficient) of the suspension is related to the transmitted light by

Equation 3-1

$$I = I_0 \exp(-\tau l) \quad (3-1)$$

Here I is the intensity of light after passing through a length l of the suspension, and I_0 is the intensity of the incident light. τ is the turbidity (or attenuation coefficient). It is important to note that turbidity is not exactly a measure of the volume concentration of the dispersed particles, but rather a measure of the total attenuating (absorbing & scattering) cross sectional area of the particles present in the beam path. This means that turbidity of the suspension with larger particle size will be higher than the one with smaller particle size, for the same number concentration. During the initial stages in the process of sedimentation, the particles will aggregate forming larger clusters, which will lead to a reduction in the attenuating cross sectional area and hence a reduction in turbidity. Furthermore, large clusters will keep settling to the bottom and hence lead to reduction in the concentration of the suspended particles, which will further reduce the total attenuating cross section area in the beam path, and hence reduce the turbidity. Also, quite obviously, the turbidity caused by particles of different materials will be different. In the following section, we will see how the rates of change of turbidity vary with various system parameters.

3.2 Results and discussion

3.2.1 Different salts and particles

The obvious parameter influencing stability that changes with change in salts or particles is the van der Waals force of attraction. As was discussed in section 1, the Hamaker coefficient depends upon the optical properties of the constituent materials in the system, i.e. the particles and the medium. Also, different materials develop different charges on the surface, but as mentioned earlier, that is irrelevant in our case. Furthermore, properties such as viscosity and density of the medium may also affect the settling rates.

Firstly, using the TBA approximation (Equation 2-5), we can estimate the approximate values of the Hamaker coefficients of different particles in different salts. These results are summarized in Table 3-1.

Table 3-1: Estimation of Hamaker coefficient of different nanoparticles in molten sodium nitrate and molten NaCl and KCl mixture

	NaNO ₃ (n~1.43)	NaCl - KCl (n~1.4)
Silica (n=1.5)	1.24 zJ	2.56 zJ
Alumina (n=1.75)	23.65 zJ	28.46 zJ
Titania, Anatase (n=2.49)	192.23 zJ	203.29 zJ

As we see, silica has the closest matching index of refraction and hence the lowest value of Hamaker coefficient in molten salts. So we expect the aggregation rate of silica to be slower than others. However we have already seen in chapter 2 that in a completely destabilized system like

molten salt, the reduction in Hamaker coefficient might not be of much great help in slowing the aggregation if only DLVO interactions dominate. However, if there is considerable hindrance to close approach of particles due to viscous or hydration interaction, then we would expect some impact of reduced Hamaker coefficient on aggregation rates.

Figure 3-3, Figure 3-4 and Figure 3-5 show the settling behavior of titania, alumina and silica nanoparticles in the Nitrate salt (NaNO_3) at 350°C and Figure 3.6 shows that of silica particles in chloride salt ($\text{NaCl} + \text{KCl}$) at 750°C . In all the cases the nanoparticles aggregated and settled in a matter of few hours, as was predicted. There was no apparent difference in the rates of aggregation of different particles in different salts.

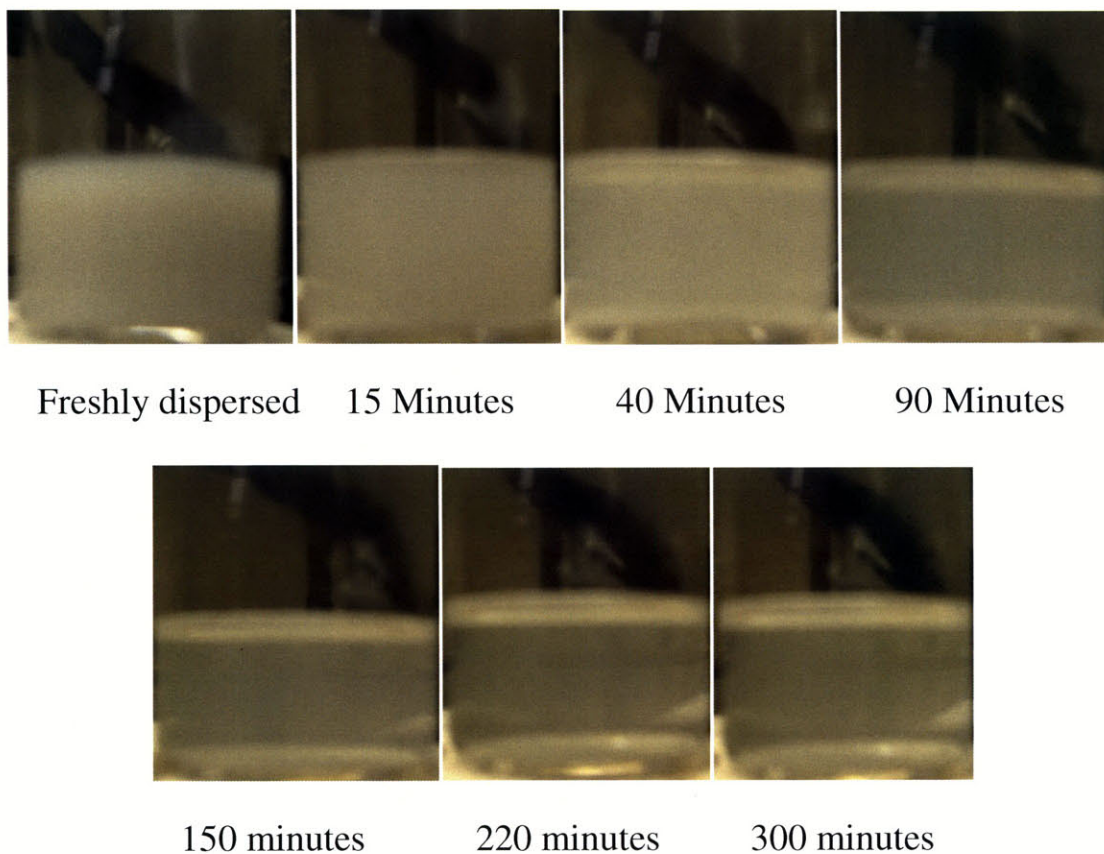
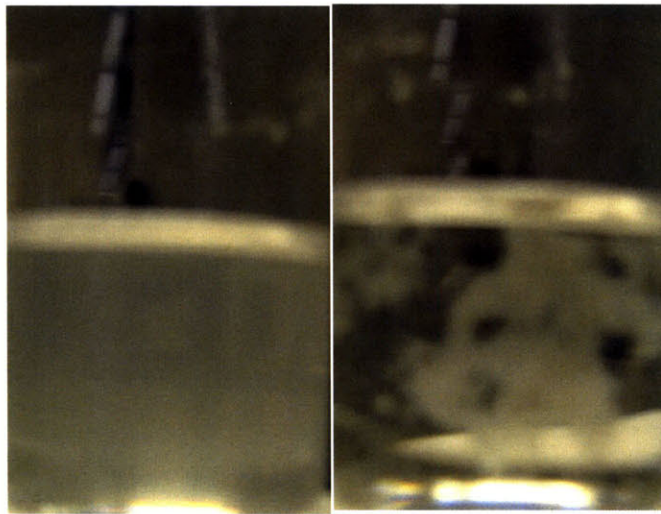


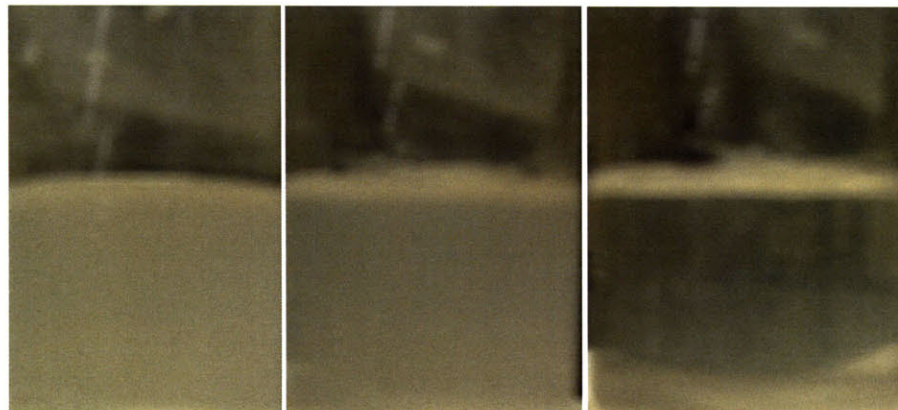
Figure 3-3: Settling of 0.1 wt% titania nanoparticles in molten sodium nitrate at 350°C .



Dispersed

40 minutes

Figure 3-4: Settling of 0.1 wt% silica nanoparticles in sodium nitrate AT 350 °C. The aggregation is seemingly faster than that of titania in molten nitrate and large clusters float around in the salt.



Dispersed

30 Minutes

70 Minutes

Figure 3-5: Settling of 0.1 wt% alumina nanoparticles in molten sodium nitrate salt at 350 °C.

It must be noted that the pictures are just representative and do not directly speak for the degree of colloidal stability of each material in that particular medium. Many factors have to be looked into before that judgment could be made. A very small amount of titania causes a lot of turbidity

in the suspension, which can be the reason for its lasting presence in pictures. The same concentration of alumina or silica might appear transparent, and hence the rates of sedimentation of different particles cannot be compared directly by these tests. However, the tests enable estimation of the sedimentation rate for a given particle/molten-salt system.

One important thing to notice is the method of aggregation of silica nanoparticles. Sodium nitrate at 350 °C has density (1.9 g/cc) very close to that of silica (2.2 g/cc). This gives rise to very large clusters of silica floating around in the suspension. For alumina and titania, the larger clusters settle out at the bottom and escape from the aggregation zone, leaving behind small particles in the suspension. On the other hand for silica, large particles continue to be a part of aggregation process which can lead to very high collision rates. We can recall from chapter 2 that collision rates are proportional to the sizes of the colliding particles. This could be one possible reason for silica to show a faster rate of aggregation.

The behavior of silica particles in the chloride mixture at 750 °C is depicted in Figure 3-6. It is interesting to see that the turbidity caused by silica nanoparticles in this medium is much higher than in pure nitrate salt. Also, although some clusters can still be seen floating around, the behavior over a period of time clearly differs from that in nitrate salt, where practically no sedimentation occurs and the entire mass floats around in the bulk. Also, the time scale of aggregation here is much like that for titania in nitrate salt. The density of NaCl + KCl mixture is ~1.6 at 750°C. So the result is consistent with the hypothesis suggested above. Since in this case the density difference between the particles and the medium is not very small, larger silica clusters settle out and escape the aggregation field, as a result of which the overall time for aggregation and sedimentation is much larger.

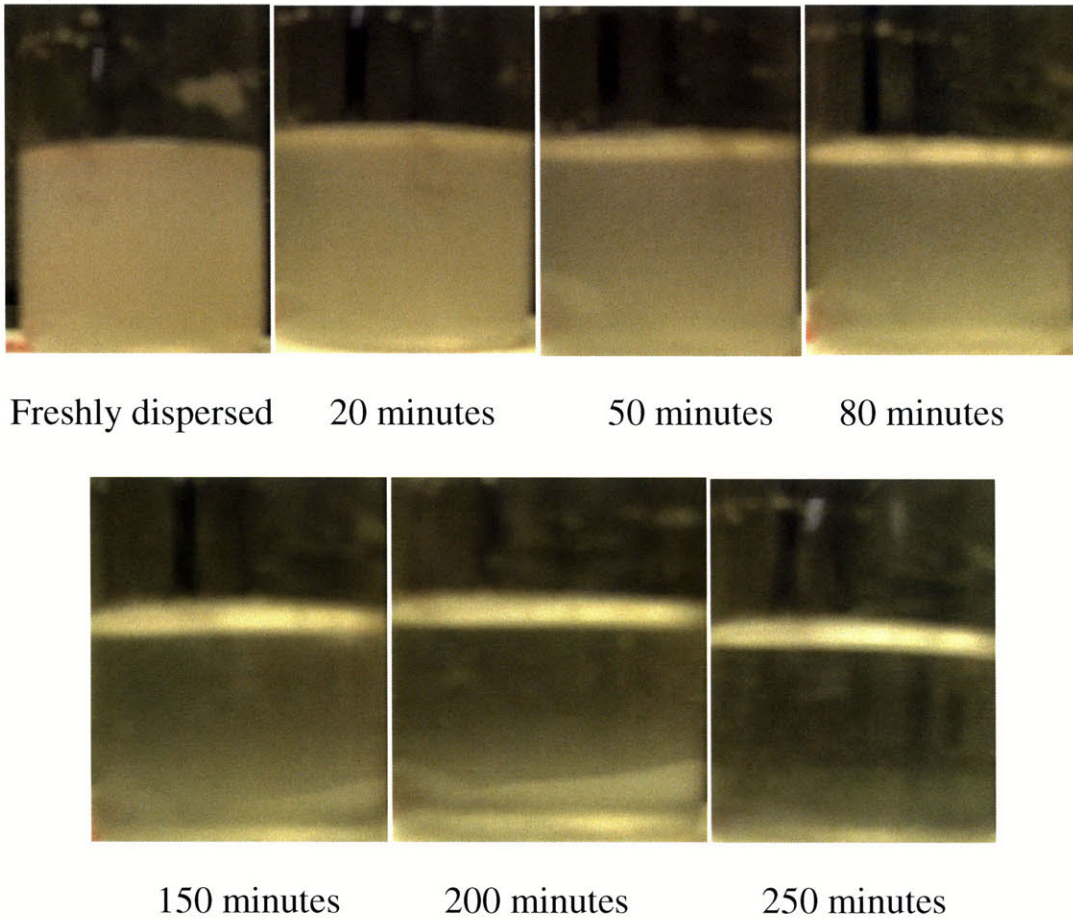


Figure 3-6: Settling of 0.1 wt% silica particles in NaCl-KCl mixture at 750 °C. The turbidity caused by silica particles in chloride salt is very high compared to that of silica particles in nitrate salt. Also, large floating clusters of silica seen in nitrate are not seen in chloride.

All in all, as of now, we can see that all three materials have poor colloidal stability in molten salts and settle out in a matter of few hours. There is no apparent reduction in aggregation rate with the changing Hamaker coefficient. Of course, with the above observation alone we are not in a position to make a definitive claim about it. However, just the fact that silica aggregates more quickly than does titania in some cases shows that the dependence of aggregation rate on other parameters is likely to be much higher than that on the Hamaker coefficient.

3.2.2 Turbidity measurement experiments

We now consider the turbidity measurements using laser attenuation for these nanoparticles in molten sodium nitrate at 350 °C. A representative example is shown in Figure 3-7. As we see, the variation of intensity received with time is linear and saturates after some time. Ideally, the saturation would represent that all the particles have settled out. However, because of the limitation of the receiver, the maximum intensity recorded is not the intensity of the incident laser. The detector saturates at an intensity of ~63800 counts, which is reached when the particles are still in suspension. Also, in nitrate salt, the turbidity introduced by silica and alumina is much less as compared to an equivalent concentration of titania. Hence, the detector reaches the saturation at a much earlier stage in the process of aggregation in the case of silica and alumina. Figure 3-7 and Figure 3-8 show the variation of the transmitted laser intensity with time for 0.01 wt% titania and alumina suspensions respectively. Note that the Y-axis has been scaled by 1000 times in the Figures, and hence the saturation value of the detector is 63.8. This line representing saturation of receivers has been marked in the Figure 3-7. As stated earlier, the two curves cannot be compared with one another, as the attenuation due to titania is significantly different from that due to alumina.

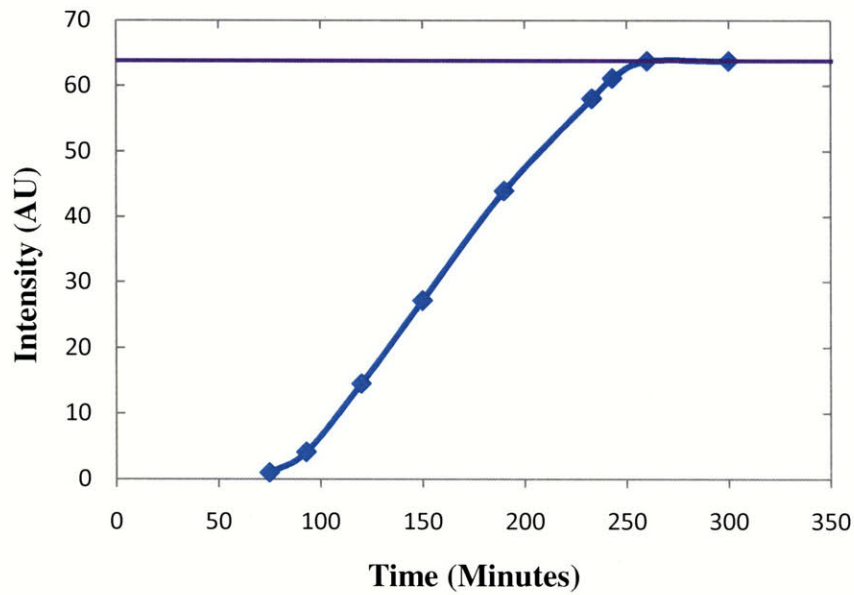


Figure 3-7: Variation of the transmitted intensity with time for a suspension of titania nanoparticles in molten sodium nitrate at 350 °C. Initially, there is no signal due to the high turbidity of the suspension. Once the signal is obtained, it varies linearly with time, until the turbidity is low enough that the receiver saturates.

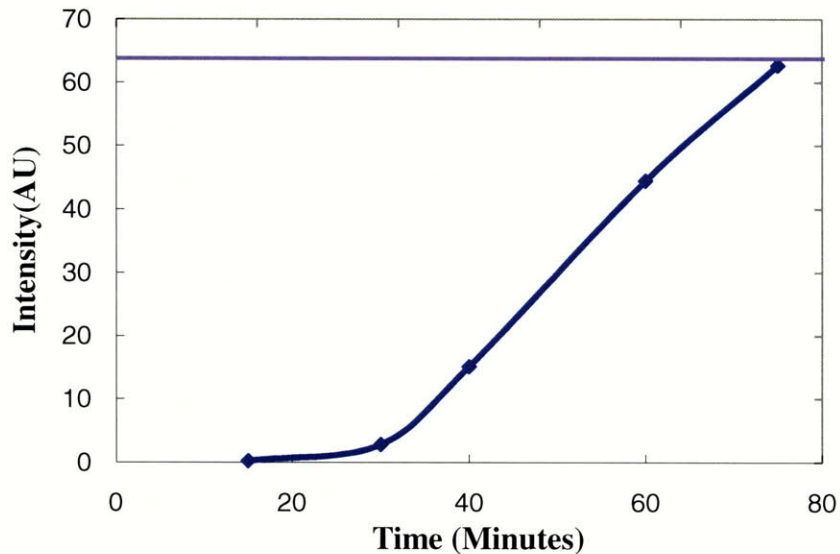


Figure 3-8: Variation of transmitted intensity with time of molten sodium nitrate with suspended alumina nanoparticles at 350 °C. The trend is very similar to that for titania nanoparticles but the attenuation caused by alumina nanoparticles is far less than that caused by titania nanoparticles.

silica suspensions reached their saturation values in a very short time (<10 minutes), and hence these results have been omitted here. It is possible to carry out these experiments for relatively non turbid particles like silica, by attenuating the intensity of the laser beam before it interacts with the suspension, or having a detector with higher saturation value.

Coming back to Figures 3-7 and Figure 3-8, a very interesting feature of the curves is that they are extremely smooth and linear until the detector saturates. The threshold value at the start arises because the laser is unable to penetrate the turbid suspension initially. We cannot claim with certainty what the behavior would be in those two regions. The details in the regions before the threshold and after saturation could be worked out with more sophisticated experiments. For the moment, we will restrict ourselves to the linear region of the curve and say that the slope is an indicator of the rate of sedimentation of particles.

Recalling that the transmitted intensity and turbidity are related by Equation 3-1, we can now find out the variation in turbidity, i.e. the attenuating cross section area with time. This relation for 0.01 wt% titania nanoparticles in molten sodium nitrate at 350 °C is depicted in Figure 3-9. It is a plot of $-1/l \cdot \log(I/I_0)$ with time. The detector saturation value is taken as the incident beam intensity I_0 . The length of beam path is taken as the inner diameter of the crucible used, which was 3.5cm. It must be noted that the values on the Y-axis do not mean much in the absolute terms, because the denominator I_0 that we have used is not the actual incident intensity but the intensity at which the receiver saturates. The purpose of Figure 3-9 is just to show the trend of the variation.

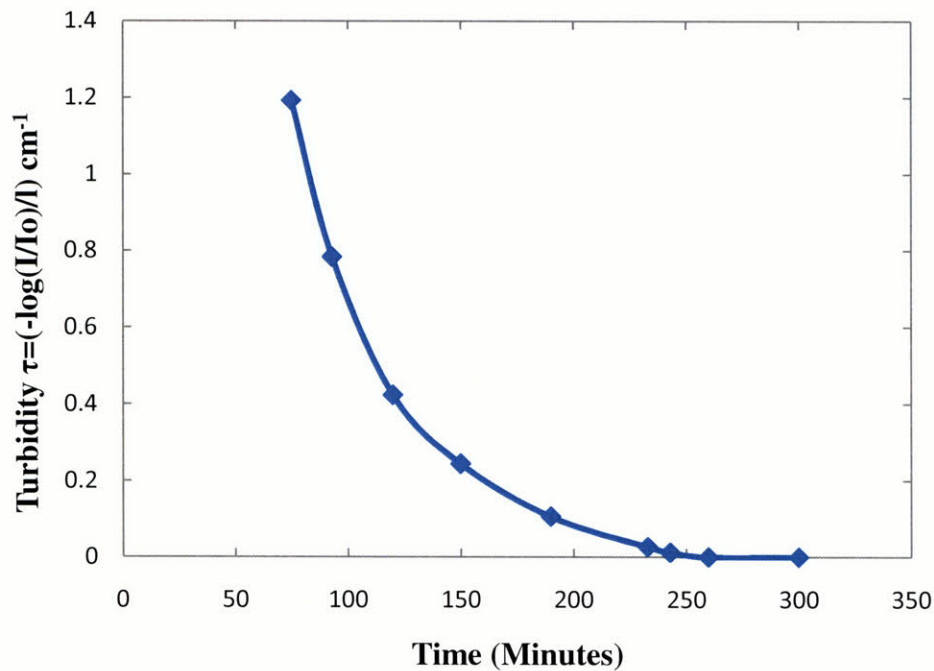


Figure 3-9: Variation of turbidity with time of a suspension of titania nanoparticles in molten sodium nitrate. The turbidity sees an exponential decay with time.

As we can see, a very smooth exponentially decaying curve is obtained. Again, it is important to note that the turbidity decreases with decreasing concentration (due to sedimentation) and also due to decreasing cross sectional area (due to agglomeration of small particles to form bigger particles). It is indeed very interesting that the net results of these two phenomena are such that it results in a linear variation of transmitted intensity with time.

At this time, we can go back to the Smoluchowski equation and see what the variation in the cross sectional area and intensity will look like if there was no sedimentation at all and particles agglomerated due to random Brownian motion. We expect this to be the case in the initial stages of agglomeration assuming that the particles follow lognormal distribution, K.W. Lee⁶ derived an analytical solution to Equation 2-16. The solution is essentially the size distribution function for particles with a fixed volume, and is shown in Equation 3-2

$$n(v, t) = \frac{N}{3\sqrt{2\pi} \ln \sigma} \times \exp \left[\frac{-\ln^2 \left\{ \frac{v}{v_g} \right\}}{18 \ln^2 \sigma} \right] \times \frac{1}{v} \quad (3-2)$$

Where $n(v,t)dv$ is the size distribution function and provides the number of particles with volume between v and $v+dv$ at time t , $v_g(t)$ is the number of median particle volume and $\sigma(t)$ is the geometric standard deviation based on particle radius. $N(t)$ is the total number of particles (which keeps decreasing with time as well). The three parameters that are required to describe the size distribution are thus σ , N and v_g . These three are given as a function of dimensionless time KN_0t by Equations 3-3, 3-4 and 3-5. K is the collision rate constant.

$$\ln^2 \sigma = \frac{1}{9} \ln \left[2 + \frac{\exp(9 \ln^2 \sigma_0) - 2}{1 + [1 + \exp(\ln^2 \sigma_0) KN_0 t]} \right] \quad (3-3)$$

$$\frac{v_g}{v_{g0}} = \frac{\exp\left(\frac{9}{2} \ln^2 \sigma\right) \{1 + [1 + \exp(\ln^2 \sigma_0)]\} KN_0 t}{\left[2 + \frac{\exp(9 \ln^2 \sigma_0) - 2}{1 + [1 + \exp(\ln^2 \sigma_0)] KN_0 t} \right]^{1/2}} \quad (3-4)$$

$$\frac{N}{N_0} = \frac{1}{1 + [1 + \exp(\ln^2 \sigma_0)] KN_0 t} \quad (3-5)$$

Using these equations, one can obtain the particle size distribution as a function of KN_0t . Now, we need the variation of the scattering cross section area with time. Using the above equations we plot the distribution of $n(r)r^2$ as a function of dimensionless size r/r_{g0} . The value of K is chosen to be $1.2 \times 10^{17} \text{ m}^3/\text{s}$, which is the collision rate constant for monodisperse particles in aqueous system at 25°C . It is also a very reasonable value of perikinetic collision rate for molten salts, as we will see later. The initial number of particles N_0 is taken as $10^{15}/\text{m}^3$, which is slightly on the conservative side for our molten salt system (0.01 wt% TiO_2 in molten sodium

nitrate converts to $\sim 10^{23}$ molecules of TiO_2 per m^3 . A 50 nm titania particle has $\sim 10^7$ molecules of TiO_2 . This gives approximately 10^{16} particles per m^3). The standard deviation of the initial distribution is taken as 1.5. The progression of the $n(r)r^2$ distribution for first three minutes is shown in the Figure 3-10.

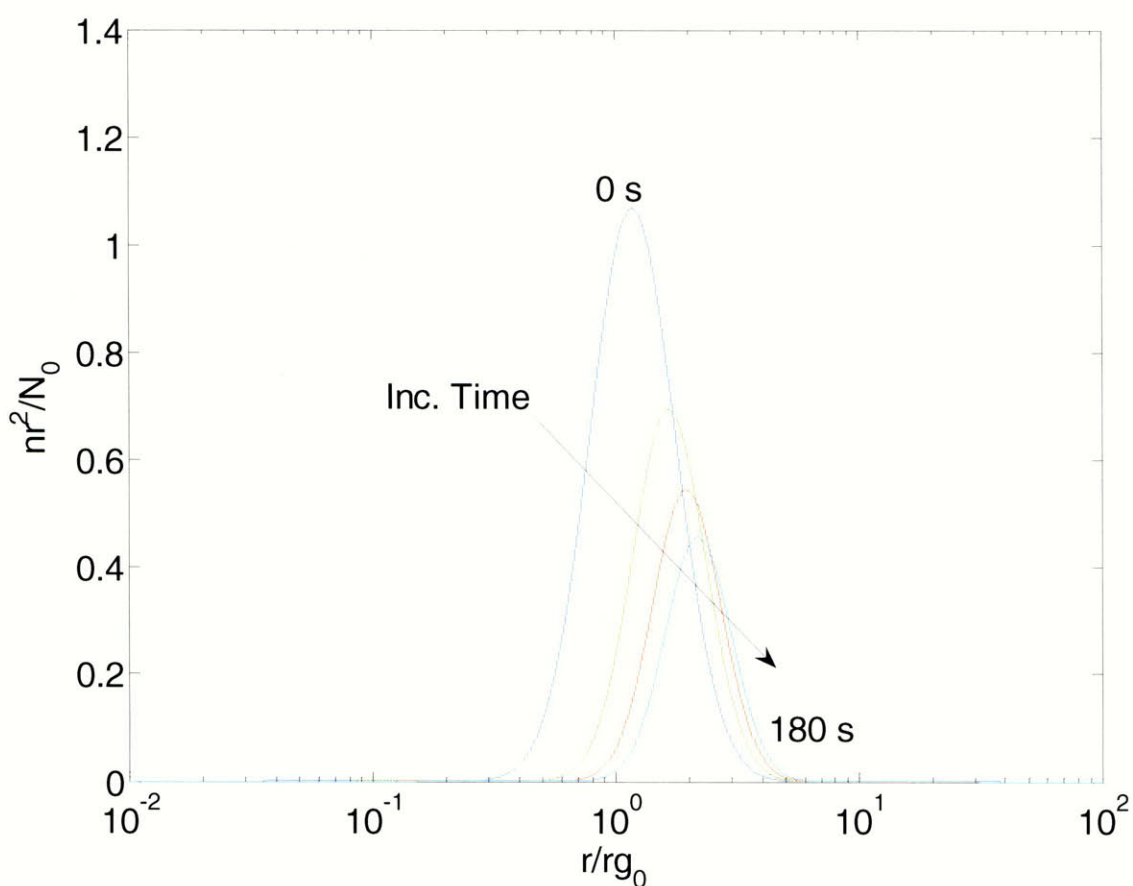


Figure 3-10: Evolution of attenuation area with time in a colloidal system aggregating due to Brownian collisions. The area under the lognormal curve at a given time represents the total attenuation area at that time.

The area under each curve (which is a measure of the total attenuation area of the colloidal system) plotted as a function of time as shown in Figure 3-1 is the expected variation in turbidity.

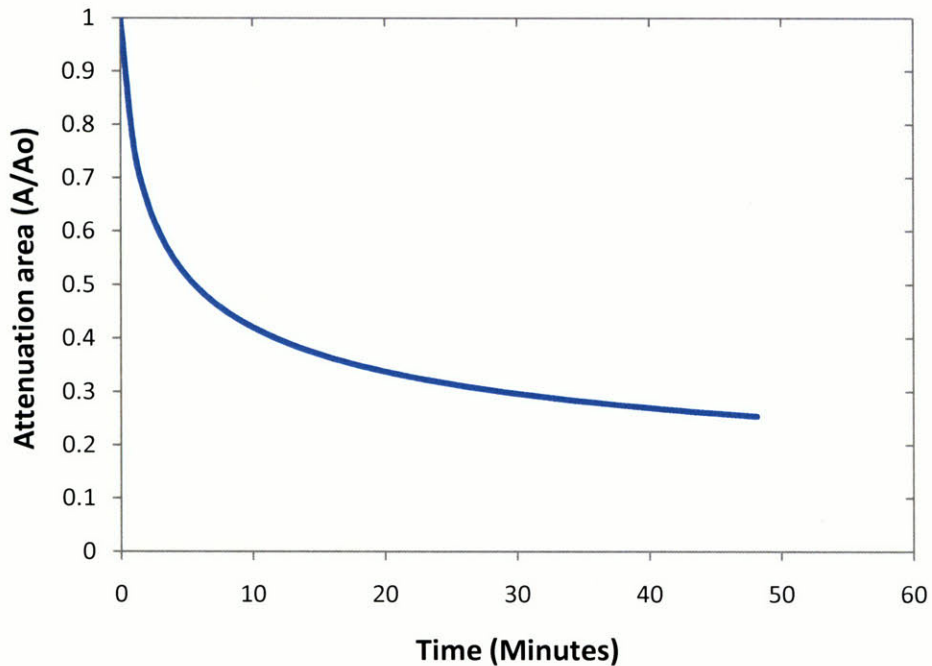


Figure 3-11: The decrease in attenuation area (or the turbidity) as a function of time, obtained by plotting the area under each curve in Figure 3-10

Finally, to see what would be the nature of transmitted intensity vs time curve for such a variation of the turbidity we just plot the $\exp(-A/A_0)$ with time. This result is presented Figure 3-12. As we see, most of the impact made by Brownian aggregation lies in the first few minutes. Also, quite clearly the curve in Figure 3-12 is not linear and that in Figure 3-11 is not as sharply decreasing as Figure 3-9. It is likely that all the information of Brownian aggregation in our experiments is hidden in the region before the threshold value. A system where aggregation might proceed with Brownian mechanism for a relatively longer time is silica in molten sodium nitrate because the densities of the two materials are comparable.

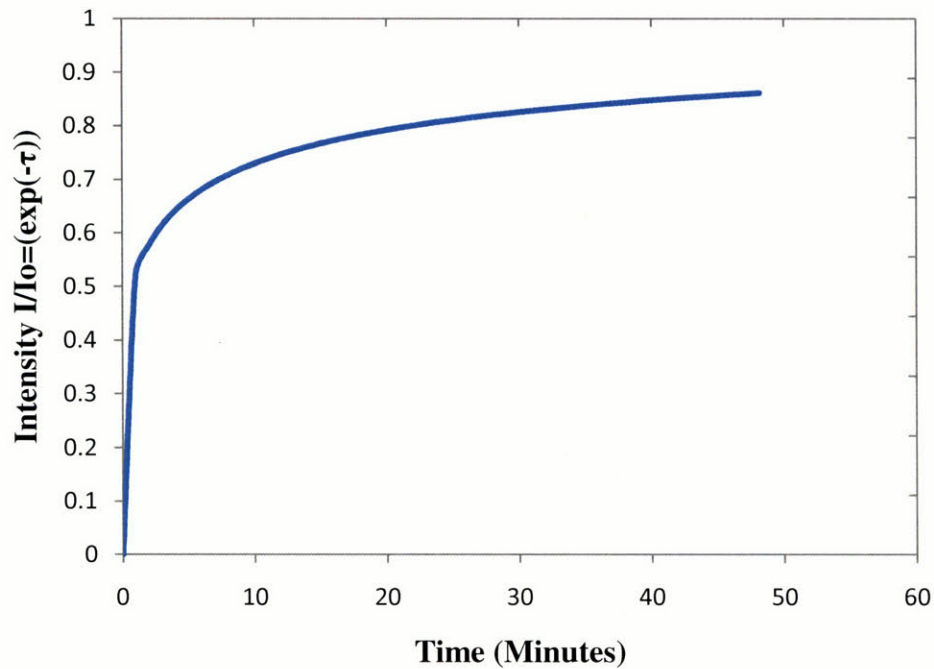


Figure 3-12: Expected variation in transmitted light with time during Brownian motion dominated aggregation. Most of the aggregation due to Brownian motion happens in the first few minutes.

More rigorous quantitative modeling is needed to understand the entire process from Brownian aggregation (or perikinetic aggregation) to gravitational sedimentation. However, we can safely assume that the initial phase is dominated solely by perikinetic aggregation whereas gravitational and density effects dominate towards the end.

We return to our turbidity measurement experiments to look at how system parameters such as particle size, temperature, initial concentration and medium impact the rate of sedimentation. Out of the materials that we have considered, titania took the longest time to reach the saturation value. Hence, titania was used as the basis material for studying the variation with particle concentration, particle size, temperature and medium.

3.2.2.1 Effect of temperature

0.01 wt% of titania was dispersed in molten NaNO_3 at three different temperatures and the change in turbidity was obtained using laser attenuation. The variation with temperature is indeed found to be very significant. At 350 °C, the saturation value was reached after ~250 minutes, whereas it reached this value in less than 100 minutes when the temperature was 450 °C. The results are shown in Figure 3-13.

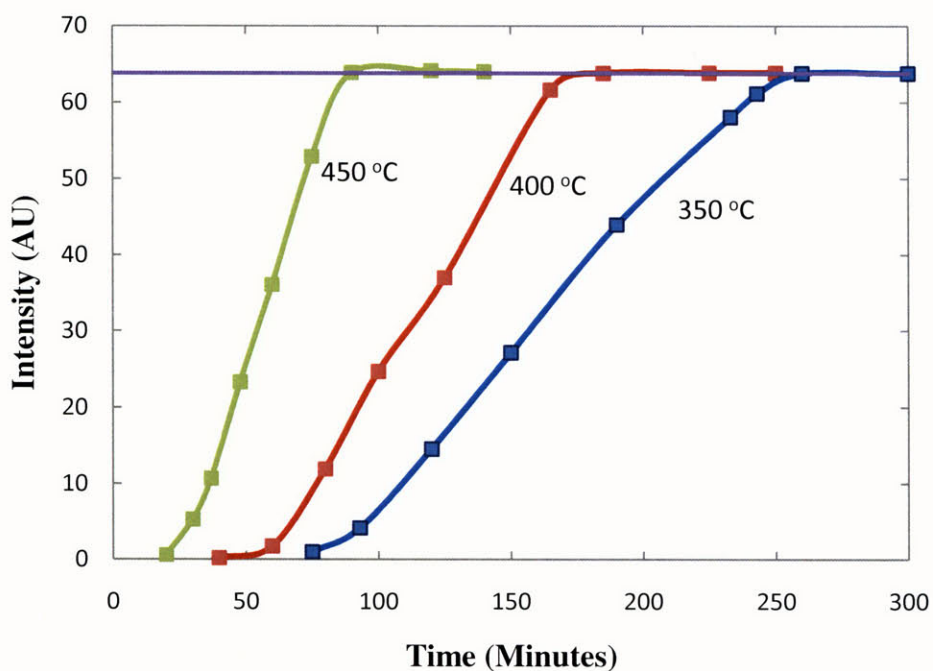


Figure 3-13: Transmitted intensity vs time for titania nanoparticles dispersed in molten sodium nitrate at three different temperatures. The threshold value for signal decreases and the slope of the linear regime increases with temperature. There is a significant variation (increase) in the total aggregation rate with temperature.

Temperature can affect the sedimentation rate in several different ways. Firstly, increasing temperature increases the thermal energy (kT) of nanoparticles and hence increases the

perikinetic collision rate constant given by Equation 2-17. Furthermore, increasing temperature decreases the viscosity and the density of the medium. Reduced viscosity increases both the perikinetic and differential settling rate constant, whereas reduced density also increases the differential settling rate constant.

The density, viscosity and perikinetic collision rate constant given by Equation 2-17 are determined for sodium nitrate at 350 °C, 400 °C and 450 °C are shown in the Table 3-2

Table 3-2: Variation of viscosity, density and perikinetic collision constant in NaNO₃ with temperature.²

Temperature °C	Viscosity μ (cp)	Density (g/cc)	K (m ³ /s) ($8kT/3\mu$)
350	2.3818	1.8745	9.20×10^{-18}
400	1.8403	1.8030	1.28×10^{-17}
450	1.4752	1.7673	1.746×10^{-17}

It is important to note that we have used the viscosity of pure molten sodium nitrate in Table 3-2, but strictly, the viscosity of the suspension should be used. As we can see, the collision rate constant varies significantly with temperature, mainly due to the variation of viscosity with temperature. The collision rate constant for 450 °C is almost twice that at 350 °C, which explains to some extent the behavior seen in Figure 3-14. Moreover, a significant decrease in viscosity will also mean that the settling due to gravity is enhanced, leading to a further increase in sedimentation rate. Thus, it seems that variation of viscosity and density of molten sodium nitrate with temperature is the main reason for the observed behavior. However, there could be other factors combining together to give such a stark variation in settling rates with temperature.

3.2.2.2 Effect of temperature gradient

The effect of temperature is considerable, so it is worthwhile to study this phenomenon in more detail. One of the interesting things to look into would be aggregation behavior in a temperature gradient. A temperature gradient was created by placing the fused quartz crucible containing molten sodium nitrate with freshly dispersed silica nanoparticles close to one of the walls of the heater. When measured, the temperature at the end close to the wall was found to be 450 °C, whereas that on the diametrically opposite face was found to be 350°C.

Quite interestingly, the silica particles overwhelmingly preferred the region close to the wall of the heater for agglomeration. The effect is indeed stark, as the salt in the low temperature region is totally clear and free of silica clusters. This effect was best captured for silica particles, because even extremely large clusters tend to float around in the medium for a long time and do not settle at the bottom, mainly due to the comparable density of silica clusters (2-2.4g/cc) and of the molten sodium nitrate (1.9 at 350 °C). It is important to note that the effective density of open nanoparticle clusters will be even less. Figure 3-14 demonstrates this result. The crucible on the left contains pure molten salt, which is placed alongside the suspension in order to compare it with the left (cooler) end. As it is evident, virtually no nanoparticles remained on the cooler side, leaving behind no doubt as to their preference to form clusters in the high temperature region. Alumina and titania particles were also found to sediment close to the hotter side.

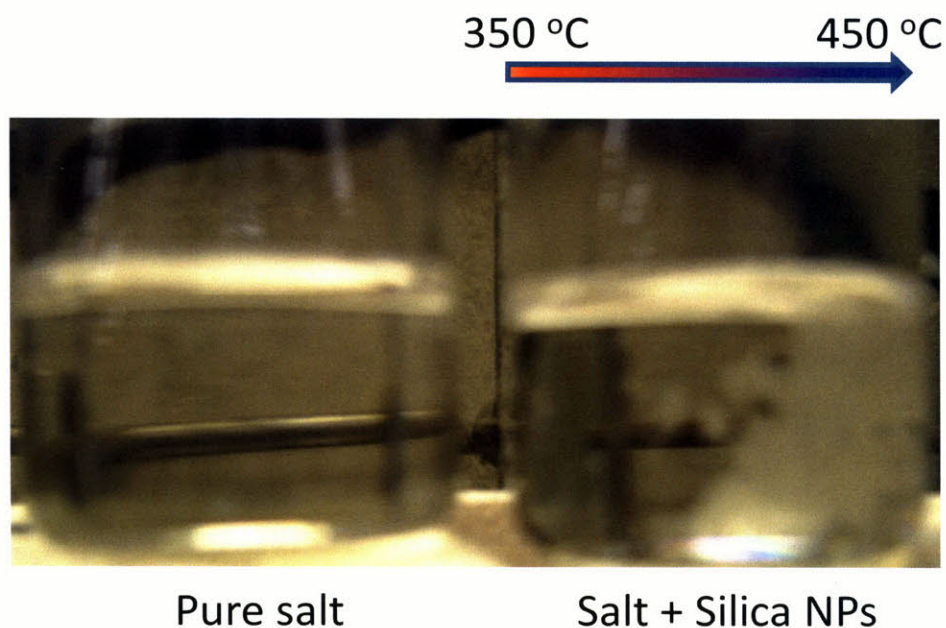


Figure 3-14: Effect of temperature gradient on aggregation of nanoparticles. The nanoparticles aggregated close to the hotter end.

It is likely that several factors are behind this interesting result. As seen before, higher temperature will lead to higher collision efficiency which could lead to formation of clusters in that region. The nanoparticles could also be driven to the high temperature end due the phenomenon of thermophoresis, although the convective flows (which would tend to homogenize the particle salt mixture) are typically a stronger transport mechanism than thermophoresis. In a liquid, normally one would expect homogenization in the distribution of particles because of convective mixing, which makes this result very interesting.

3.2.2.3 Effect of particle size

Initial particle size may play an important role in both the aggregation and the sedimentation rate. Figure 3-15 shows the comparison of sedimentation rates of commercial titania nanoparticles with sizes ~25 nm and ~100 nm respectively. The concentration of the particles was

0.1 wt% in both the cases. Interestingly, the suspension with larger sized particles crossed the threshold later than did the suspension with the smaller sized particles, but then settled at a faster rate (with a greater slope). In this particular case, the difference was small and within the range of experimental error. It is likely that initial particle size has very little impact, if any, on the rate of settling of the nanoparticles. This can be the case because initial Brownian aggregation is so fast that the difference in initial particle size becomes irrelevant.

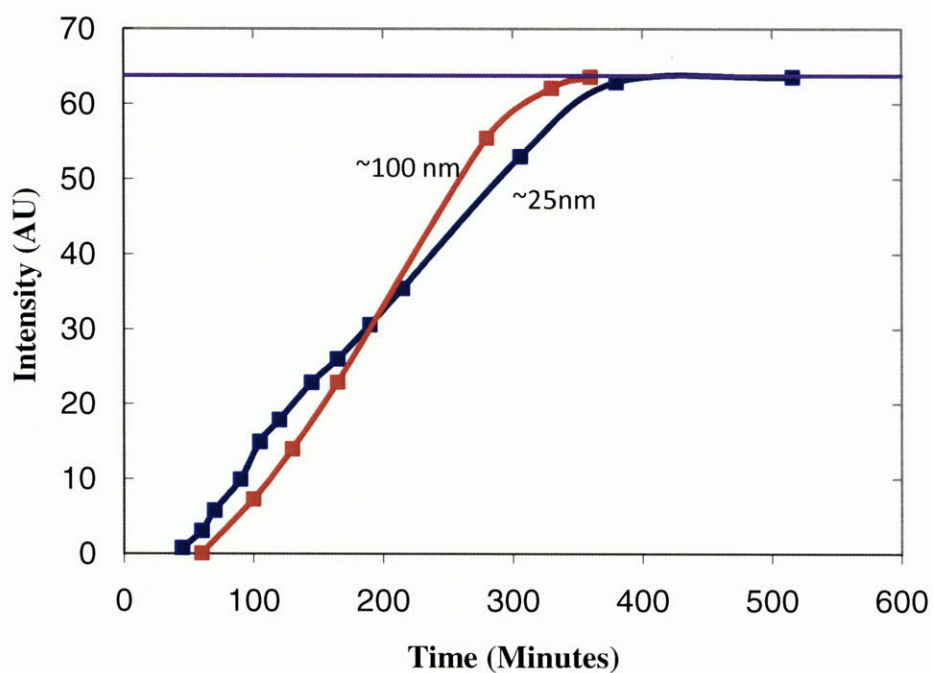


Figure 3-15: Transmitted intensity Vs time curves for different sized titania nanoparticles in molten sodium nitrate at 350 °C. There seems to be no significant effect on the aggregation rate with the change in particle size.

3.2.1.2 Effect of concentration

Initial concentration is an important parameter in determination of aggregation kinetics. The number of collisions taking place is directly proportional to the number of particles present in the system. Hence, the aggregation rate should be much faster in the suspension with the higher

particle concentration. Figure 3-16 presents the turbidity curves for initial concentrations of 0.1 and 0.01 wt% respectively. The result is indeed interesting. The suspension with lower initial concentration reaches the threshold after the higher one does, which means that the attenuating cross sectional area of the higher concentration suspension is less than the one with lower concentration suspension at that particular time (in absolute terms). It should be noted that the higher concentration suspension had ten times the attenuating cross section area to begin with. It intuitively makes sense that due to high concentration and increased number of collisions, the aggregation rate is much higher and hence the lower concentration suspension remains suspended for a longer time. However, this trend does not continue far beyond the threshold point, and the slope of the transmitted intensity vs time curve for high concentration particles is smaller than that with low concentration particles. These trends are depicted in Figure 3-16 A. Figure 3-16 B shows the turbidity vs time curves for these two different concentrations which conveys the same information.

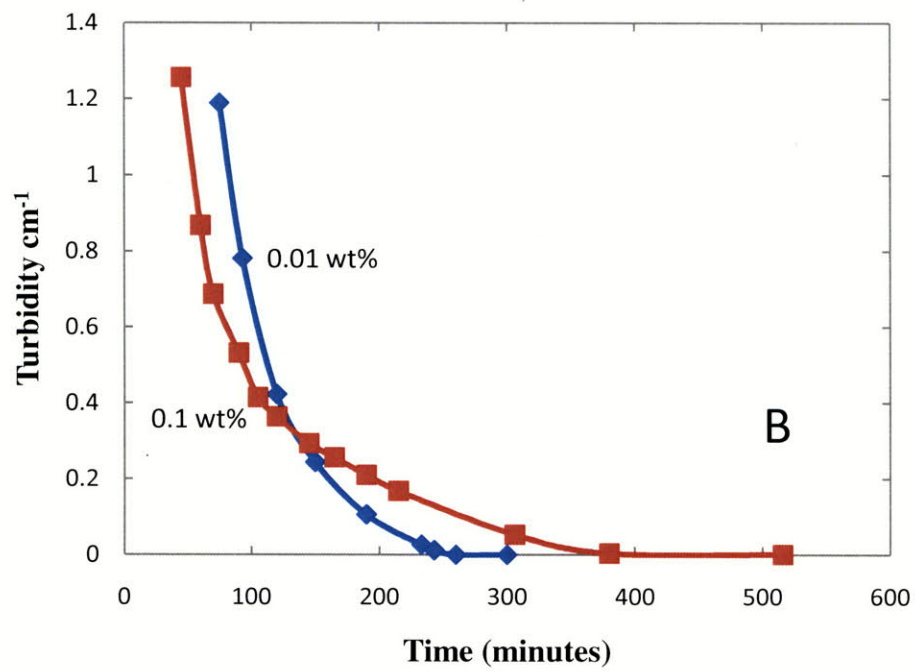
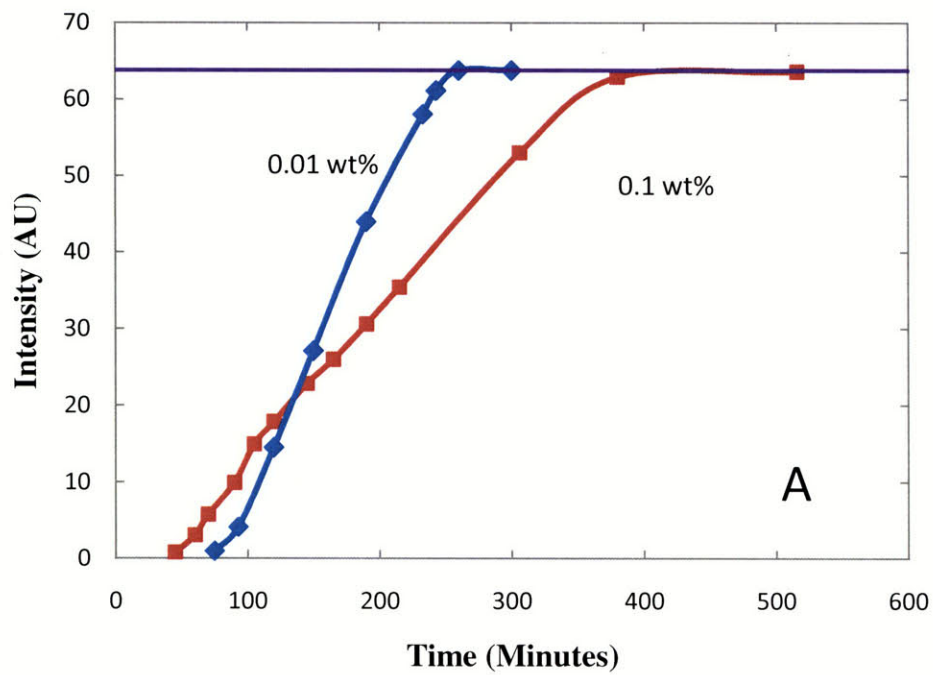


Figure 3-16: Transmitted intensity Vs time (A), and turbidity vs time (B) curves for titania nanoparticles in molten sodium nitrate at 350 °C for two different concentrations.

It is difficult to reason out such an intersection of the two curves based on the concepts discussed in chapter 2. It suggests that if an infinitely powerful source of light was used and turbidity measurements were carried out from the starting point where the nanoparticles were fully dispersed (rather than from threshold point), then the curves would not have followed the extrapolation of the smooth linear behavior that they show. This could be claimed because at time $t=0$, the turbidity of the higher concentration suspension needs to be 10 times higher than that of the lower concentration suspension which clearly will not be the case if the two linear lines are extrapolated to the starting point $t=0$. Thus, it is evident that the difference in threshold value is due to the difference in rates of perikinetic aggregation early on. However, it is not very clear as to why the rate of aggregation becomes faster in the lower concentration suspension towards the later stages.

3.2.2.3 Effect of medium of dispersion

Finally, we must also take into account the effect of varying the medium of dispersion on the colloidal stability of the nanoparticles. 0.01 wt% titania nanoparticles were dispersed in molten NaNO_3 at 350 °C and molten $\text{NaCl} + \text{KCl}$ mixture at 750 °C, and the measurements of transmitted intensity versus time are shown in Figure 3-17. Once again, it was observed that the two curves cross each other. The suspension with nitrate salt reached the threshold point later than that with the chloride salt, but it reached the saturation point before the chloride salt suspension did. This is perhaps an indication that initial aggregation controlled by Brownian dynamics is faster in chloride salt whereas the aggregation rate becomes faster at a later stage when gravity and differential settling start dominating. The viscosity of an NaCl-KCl molten mixture is about 1.5 cp at 750 °C (compared to 2.3 for nitrate salt at 350 °C) and hence lower viscosity and higher temperature will yield a much higher perikinetic rate constant. Also, the

density of the chloride salt is lower, which implies higher differential rate sedimentation as well. In that case there is no apparent intuitive reasoning to explain the result, and more detailed investigation will be required to understand this behavior better.

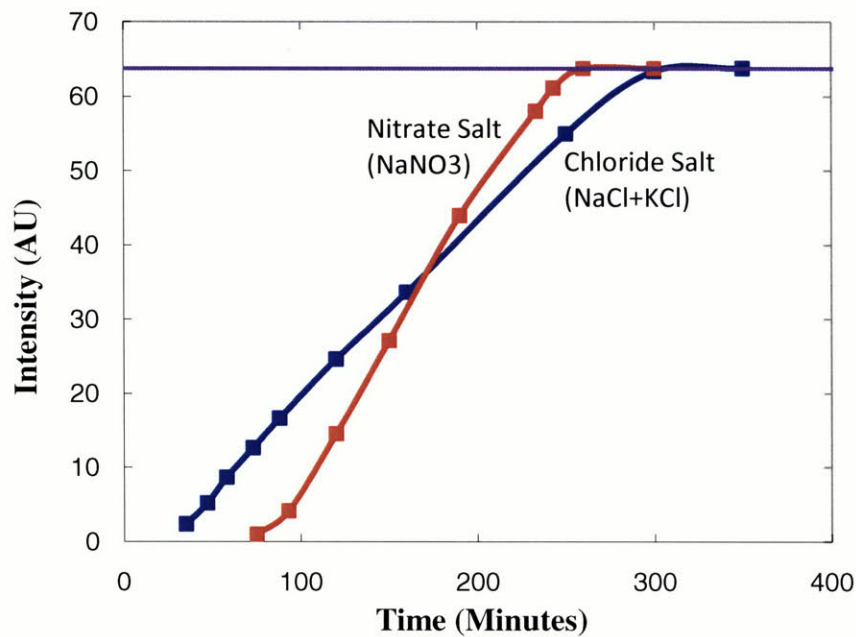


Figure 3-17: Effect of different media on the sedimentation rates of nanoparticles. The high temperature chloride suspension reached the threshold value before the nitrate but ended up taking more time to reach detector saturation point.

3.3 Summary

We have seen that nanoparticles settle within a matter of few hours in molten salt, and constant agitation will be required if particles are to be kept suspended for any possible application. The aggregation rate does not depend significantly on the Hamaker coefficient of the nanoparticles in the molten salt medium, and other factors such as viscosity and density of the medium have a

greater influence on the kinetics of aggregation and deposition. The parameter that was found to have the most profound impact on the settling rates of nanoparticles is temperature. The particles settled much more rapidly at higher temperatures. In fact in a temperature gradient, the particles tend to cluster together, agglomerate and deposit closer to the hotter side. The cursory study of kinetics of aggregation and deposition of nanoparticles in molten salts indeed provides some interesting results each of which need to be explored in much greater detail through more sophisticated and sensitive experiments. Also, rigorous mathematical models will need to be developed that can reconcile the theory with observations. In short, much can be done to further explore the area of kinetics of aggregation and sedimentation of nanoparticles in molten salts.

However, we have found out that none of the suspensions is likely to be stable for a long time and continuous agitation will be required. Instead of going into more detail on the kinetics of aggregation, we will explore in chapter 4 the possibility of designing engineered nanoparticles that may be stable in the molten salts for a long time.

3.4 References

1. Lee, K. W., Change of particle size distribution during brownian coagulation. *Journal Of Colloid And Interface Science* 1983, 92, (2), 315-325.
2. Janz, G. J., *Molten salts handbook*. Academic press: New york, 1967.

4. Potential stabilization of nanoparticle suspensions through ultra-low Hamaker coefficients

So far we have seen how molten salts form a very unfavorable medium for colloidal stability of nanoparticles. Screening of coulombic charges due to the ionic medium and prohibition of polymeric surfactants due to extreme temperatures make it virtually impossible to have a colloidally stable system of nanoparticles in molten salts. We have seen that aggregation and sedimentation of nanoparticles in this medium occurs rapidly. We have studied the effects of various parameters such as concentration, temperature, nanoparticle type and molten salt on aggregation rate. We have found experimentally that the variation of aggregation and deposition rate with temperature is most significant. While variation in physical parameters like density and viscosity can explain some of the trends, more work needs to be done to quantitatively explain all the trends observed in chapter 3.

Instead of studying the kinetics of aggregation in molten salts in further details, we will move our attention to a very interesting problem, which is development of a kinetically stable system of nanoparticles dispersed in molten salt. We will explore the theory to determine if it is theoretically possible to find a salt and particle system which will show long term stability, just like low temperature nanofluids that are being developed and used for applications. The only way to stabilize nanoparticles is to ensure that collisions don't lead to sticking. In conventional nanofluids, this is done by electrostatic repulsion or steric hindrance. As we have shown earlier, relying on electrostatic or steric stability will not work in our system. Hence, we need to make sure that the van der Waals interaction energy between the particles in contact is sufficiently small that the thermal energy of particles undergoing random Brownian motion is sufficient to

keep the particles apart. It must be noted that in any general colloidal system, there is nothing apart from the van der Waals force that causes the particles to attract one another. Hence, if there were no van der Waals forces at all, every colloidal suspension of nanoparticles would remain stable.

We come to an important point of discussion. How small should the Hamaker coefficient be in order to make the Brownian forces stronger than the van der Waals forces? When two particles are in contact, the distance between them is zero and according to Equation 2-3, the van der Waals force of attraction should be infinite. In that case, anything more than absolute zero value of the Hamaker coefficient will lead to infinitely strong attraction at contact, and there would be no hope of any stabilization whatsoever. As we will see shortly, a zero value of Hamaker coefficient between the particles in a particular medium is virtually only possible when the two materials are exactly the same. However, a very small value of Hamaker coefficient can also do the trick for us. In chapter 2, we discussed the fact that the van der Waals interaction energy does not go to infinity even when the particles are in apparent physical contact. This is because the distance between the particles does not really go to zero. At very close separations, short range Born repulsions become dominant and keep the two particles separated by an equilibrium distance of approximately 0.1-0.2 nm.¹ Generally, 0.165 nm is taken as the mean equilibrium distance between surfaces in contact.²

Now, for spheres of equal radius, van der Waals energy at very close approach is given by³

$$U = \frac{A}{12} \left(\frac{d}{l} \right) \quad (4-1)$$

Here, as before, A is the Hamaker coefficient, d is the diameter of the spherical particles and l is the distance between the particles.

If $U_{\text{contact}} \ll kT$, the thermal energy of the particles will be sufficient to keep the van der Waals forces at bay, thereby preventing agglomeration. A short note here is important to avoid confusion. In the traditional DLVO theory, we said the thermal energy should be less than the maximum of the DLVO potential for colloidal stability, thereby preferring low thermal energy for stability. Thus, higher temperatures were detrimental to colloidal stability. On the other hand, in our case we want the thermal energy to be larger than the Hamaker coefficient, which suggests that higher temperatures are favorable for colloidal stability. At first, these may appear as contradicting, but actually they are not. In general, the well to the left of the DLVO energy barrier (primary minimum) is infinitely deep and hence once the particle enters the well, the thermal energy is not sufficient to separate them again. On the other hand, with finite distance of contact, if the van der Waals interaction is made extremely small ($\ll kT$), the thermal energy will be sufficient to keep them apart and prevent their agglomeration. Now we can work out a quick order of magnitude calculation and estimate how small should the Hamaker coefficient be. We are basically looking at the point where the van der Waals energy at “contact” becomes much less (say ten times less) than the average thermal energy kT .

The value of kT at 500°C is 1.06×10^{-20} J, or 10.6 zJ (zepto Joules). Let us assume that we need the thermal energy to be 10 times greater than the van der Waals energy at contact. Hence, $U_{\text{contact}} \sim 1$ zJ. If we assume the size of the particles to be 15 nm and the distance separating them to be 0.16 nm, then $d/l \sim 0.01$. Hence, $A \sim 0.1$ zJ. This gives us the approximate value of the Hamaker coefficient which will be small enough for the particles to be stabilized merely due to the thermal energy.

This value of Hamaker coefficient is indeed extremely small which is practically unrealizable for most combinations of materials for suspension media and nanoparticles. It is now a good time to

point out once again that equation the Tabor Winterton approximation presented in Equation 2-5 for calculations of van der Waals forces using the refractive index of the interacting materials is just an approximation and is not suitable to get precise values of Hamaker Coefficients. From the Tabor Winterton approximation , we see that any two materials with exactly the same refractive index will have zero Hamaker coefficient and hence no van der Waals force of attraction. However, as we will soon discover, this will only be true when the interacting materials have the same index of refraction at all possible wavelengths (from 0 to ∞). That is, the response of the material to the electromagnetic waves will be same for all the wavelengths. This essentially means that the Hamaker coefficient will be zero when the two materials are exactly the same. In this chapter, we will look into the detailed theory behind the calculations of Hamaker coefficients and look into the feasibility of obtaining the ultra low values of Hamaker coefficients that we are looking for.

4.1 Modern theory to estimate Hamaker Coefficient (Lifschitz formulation)

As stated before, although the Tabor-Winterton approximation does give us a fair general idea most of the time, it is by no means an exact expression. In order to rigorously calculate the Hamaker coefficient (which is essential in our case), one needs to know the optical dispersion (or absorption) properties of the particles and the medium at all wavelengths. Lifschitz developed the modern theory⁴ to estimate the Hamaker coefficient in terms of the optical properties of all the materials involved in the medium.

4.1.1 The data required for calculation of the Hamaker coefficient using Lifschitz formulation

Before going into the details of the Lifschitz formulation, let us first look into the data that are required for calculation of the Hamaker coefficient. We need to get the variation of imaginary part of the dielectric constant ϵ'' with frequency ω , and this can be obtained from several other optical properties. These optical properties are complex quantities in which the real and imaginary parts correspond to the dispersion and absorption of light in the material. There are algebraic relations between numerous optical properties such as Index of refraction ($n+ik$), dielectric constant ($\epsilon'+i\epsilon''$), optical conductivity ($\sigma'+i\sigma''$) and interband transition strength ($J_{cv,1}+iJ_{cv,2}$). We will come across several such relations in the coming sections. Thus, if we know any one property variation with wavelength, we can obtain any other property that we are interested in, merely by mathematical transformations and algebraic calculations. In order to obtain the ϵ'' spectrum (and hence the Hamaker coefficient), we can measure any one of the above properties. The physical intuition of the optical properties being related to one another comes from appreciating the fact that all the properties are ultimately related to just the interaction of an electromagnetic wave with the electrons of the material.

Also, it is important to understand that the real and imaginary parts of any particular optical property themselves are not independent of one another, but are related by the Kramers-Kronig relationship. For example, ϵ' and ϵ'' are related by the Kramers-Kronig relations shown below in Equations 4-2 and 4-3.

$$\epsilon'(E) = 1 + \frac{2}{\pi} P \int_0^{\infty} \frac{E' \epsilon''(E')}{E'^2 - E^2} dE' \quad (4-2)$$

$$\epsilon''(E) = -\frac{2E}{\pi} P \int_0^{\infty} \frac{E'(E')-1}{E'^2 - E^2} dE' \quad (4-3)$$

Here, P represents the Cauchy principal part of the integral. There are similar Kramers-Kronig relations for real and imaginary parts of the Index of refraction etc. These relations follow from the requirement of causality, which essentially means that there can be no effect before the cause. Thus, the reflection or absorption of light by a material can only take place after the arrival of a primary light wave. The rigorous mathematical derivation of Kramers-Kronig expressions can be found in the book “*Optical Properties of Solids*” by Fredrick Wooten.⁵

4.1.1.1 Measurement of ϵ'' using experimental techniques

Various experimental techniques can be used to obtain the ϵ'' spectra that we are looking for.

Vacuum Ultraviolet (VUV) reflectance measurements can be used to obtain the optical reflectivity over an energy range spanning the visible and shallow ultraviolet regions. It measures the optical reflectance $R(E)$, which can be used to measure the phase shift $\theta(E)$, through KK transformation. R and θ can then yield the optical constants n and k (real and imaginary part of the refractive index), which can then yield ϵ'' . Similarly, spectroscopic ellipsometry measures ellipsometric parameters ψ and Δ , defined by Equation 4-4,

$$\tan(\psi)e^{i\Delta} = \frac{R_p}{R_s} \tag{4-4}$$

Where R_p/R_s is the complex ratio of the p- and s- polarized components of the reflected amplitudes with R_p and R_s representing the electric field components parallel and perpendicular to the plane of incidence respectively. These parameters can be analyzed using Fresnel equations in a computer based modeling technique to obtain the optical constants n and k .⁶ The third technique that can be used is Electron Energy Loss Spectroscopy (EELS) that determines the energy loss function ($-\text{Im}(1/\epsilon)$).⁷ These different measured parameters are then easily converted into ϵ'' using a series of mathematical relations and Kramers-Kronig transformations. Once we

have the ϵ'' , we can obtain the van der Waals spectra, which can then be used to calculate the Hamaker coefficient.

One of the most important challenges in the calculation of the Hamaker coefficient is that the ϵ'' spectrum needs to be obtained for the entire range of photon energy (0 to ∞ eV). Of course, it is impossible to get the data with precision up to ∞ eV. Most experimental techniques (Reflectivity, Ellipsometry etc.) can provide us the information in visible and near Infrared and Ultraviolet region (up to 10 eV). Electron Energy Loss Spectroscopy (EELS) can yield the information in deep UV (up to 25 eV), but cannot be performed with molten salts at high temperatures. The best method to obtain the data in the deep UV region for our system of interest (up to 35-40 eV) is the first principle calculation using the band structure of the materials. Data beyond that range are rarely required because there are hardly any excitations in materials at frequencies that high, and ϵ'' can conveniently be taken to be zero beyond 40 eV. Thus, it (40 eV) can be considered infinite for all practical purposes.

4.1.1.2 Ab Initio calculations

The input required for Ab Initio calculation of the dielectric spectrum is the location of atoms and ions in a cell and the appropriate boundary conditions. Essentially, the response of the material is obtained by quantum calculations based on the interaction of electromagnetic waves of different frequencies with the electron cloud of the material. This then gives the band structure of the material as the output which can then yield information about the response of the material to a photon of any energy. Thus, we can obtain any optical property of the material that we are interested in. Most of the computations are relatively easy for single crystal solids, which have a periodic structure that extends throughout the system. They are much more expensive for liquids,

wherein one requires a much larger super-cell of atoms for computation because of the disorder in their structure.

The main equation used to obtain ϵ'' spectra from band structure is⁸

$$\epsilon_{ij}''(\omega) = \frac{4\pi^2 e^2}{\Omega m^2 \omega^2} \sum_{kn\sigma, kn'\sigma} \langle kn\sigma | p_i | kn'\sigma \rangle \langle kn'\sigma | p_j | kn\sigma \rangle f_{kn} (1 - f_{kn'}) \delta(e_{kn'} - e_{kn} - \hbar\omega) \quad (4-5)$$

Here ϵ_{ij}'' is the imaginary part of the dielectric spectrum at a given frequency ω , with mass m , and Brillouin zone volume Ω . The momentum operators p_i and p_j operate on both the valence and conduction band wave functions, where the i and j subscripts represent the directions of the tensor in three dimensional space. The Fermi function (f_{kn}) terms ensure that only transitions between an occupied valence to an unoccupied conduction band transition are allowed, and the delta function ensures that only transitions corresponding to the particular energy $\hbar\omega$ are considered.

Many commercially available programs carry out first principle band structure calculations up to 10 eV, and most of them implement the tight binding approximation (TBA), which essentially assumes symmetrical nature of the bands. These approximations provide accurate information in the region close to the band gap of the material, but cannot be used for reliable information in the range of interest (0 to 40 eV). One of the reasons for these is that accurate response up to 40 eV is hardly required for any other purpose than calculating the Hamaker coefficients. Ching et. al. have carried out the Ab Initio calculations to determine the electronic structure (ϵ'' spectra) up to 40 eV of most ceramic materials.¹¹ They have already reported the ϵ'' calculations of various inorganic salts (in solid crystalline state) using density functional theory with an OLCAO basis.¹²

The Ab Initio calculations reported in this chapter have also been carried out by Prof. Wai Yim Ching per our request, and we are extremely thankful to him for his help.

One limitation that Ab Initio calculations have is that they just take into consideration the response of the material due to the electronic band structure and cannot obtain fixed dipole interactions. This can be of significant impact in systems with a fixed dipole moment like water, which have a very high static dielectric constant (~80 for water). These, however, are not expected to be of much impact in our system. Also, there are ways to correct for these interactions which we will briefly discuss later.

4.1.2 van der Waals – London dispersion spectra ($\epsilon(i\xi)$)

For calculation of the Hamaker coefficient, the ϵ'' spectrum needs to be converted into the van der Waals –London dispersion spectrum (vdW-Lds) $\epsilon(i\xi)$, once again through a Kramers -Kronig (KK) transformation, as shown in Equation 4-6.

$$\epsilon(i\xi) = 1 + \frac{2}{\pi} \int_0^{\infty} \frac{\epsilon''(\omega)d\omega}{\omega^2 + \xi^2} \tag{4-6}$$

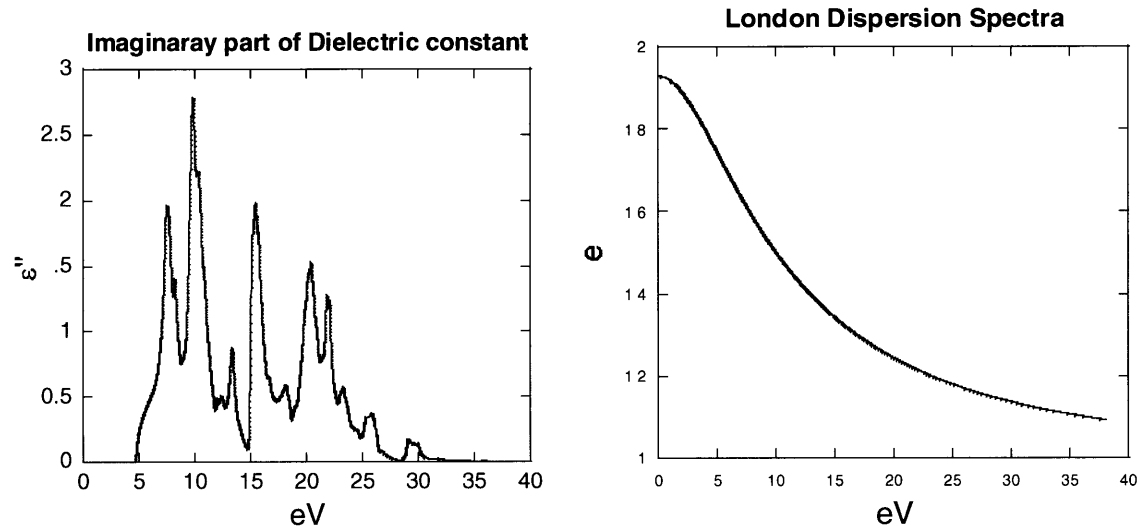


Figure 4-1: An example of conversion of absorption spectrum to van der Waals spectrum through Kramers Kronig transformation. At the top, we have the ϵ'' of solid KCl, and at the bottom, we have a converted smooth monotonic van der Waals spectrum.

The resultant van der Waals spectrum is the real part of the dielectric constant over imaginary frequencies. ξ are not ordinary sinusoidal frequencies, but are crafted in the language of exponential variations pertaining to the ways in which spontaneous charge fluctuations die at different rates. Thus, the van der Waals spectrum is an optical property that represents the retardation of oscillators. It is called a van der Waals spectrum because it is not used for any practical purpose other than for the calculation of van der Waals forces of interaction. After KK transformation, the $\epsilon(i\xi)$ behave smoothly decreasing monotonically versus frequency, without spikes of absorption or dispersion seen for real oscillations. The van der Waals spectra of the interacting species contain all the information that is required for calculation of Hamaker coefficients. The blurring of details in $\epsilon(i\xi)$ is one reason why it is often possible to compute van

der Waals interactions to a reasonable accuracy even without full knowledge of absorption spectra³.

4.1.3. Calculation of Hamaker coefficient using Hough and White approximation

The rigorous formulation to calculate the Hamaker coefficient from van der Waals spectra of the particles and the medium is fairly involved. The Hough and White approximation¹⁰ given below is a good starting point, especially to gain understanding of the areas of impact, i.e. the factors that are crucial in the determination of the Hamaker coefficient. The non retarded Hamaker coefficient between two particles of “1”, in the medium “2”, is given by

$$A = \frac{3kT}{2} \sum_{n=0,1..}^{\infty} \prime \Delta_{12}^2 \quad (4-7)$$

$$\Delta_{12} = \frac{\varepsilon_1(\xi) - \varepsilon_2(\xi)}{\varepsilon_1(\xi) + \varepsilon_2(\xi)} \quad (4-8)$$

$$\xi_n = \frac{2\pi kT}{\hbar} \quad (4-9)$$

$\varepsilon_j(\xi)$ and $\varepsilon_k(\xi)$ are read off directly from the van der Waals spectra for each term in the summation. Note that the prime symbol on the summation indicates that the first term is multiplied by half. In the summation in Equation 4-7, the sampling frequencies are evenly spaced at increments of KT/\hbar (0.16eV at room temperature). Thus, given the optical spectra (and hence the van der Waals spectra) of the nanoparticles and the medium, one can evaluate the Hamaker coefficient for the system.

Figure 4-2 illustrates the calculation of Hamaker coefficients from the van der Waals spectra. Two hypothetical van der Waals spectra are shown. Each term in the summation of equation 6 is

then obtained by just substituting the values of $\epsilon_j(\xi)$ and $\epsilon_k(\xi)$ at the values of ξ given by the Matsubara frequencies, which are represented by vertical lines in the Figure. Thus, it is evident that optical contrast between the nanoparticles and the medium has to be minimized in order to minimize the van der Waals forces of attraction. In other words, the van der Waals spectrum of the nanoparticles needs to match the medium over as large a range as possible.

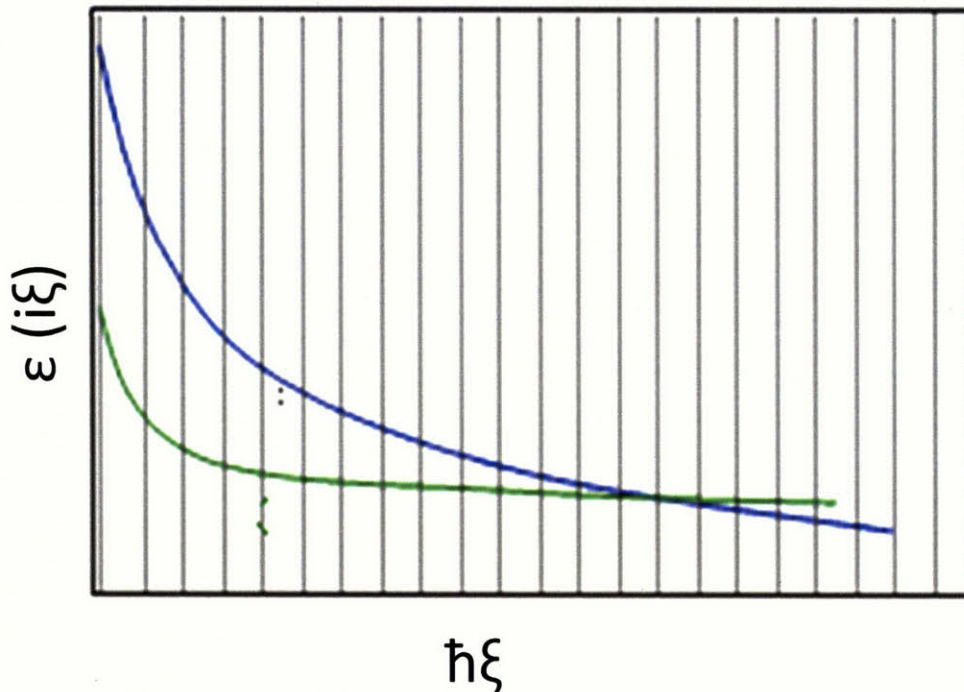


Figure 4-2: Illustration of calculation of the Hamaker coefficient using the van der Waals spectra of the materials of interest. Note that the vertical lines represent the Matsubara frequencies, over which the summation has to be carried out.

It is important to note that there are just a few terms in the summation in Equation 4-7 belonging to the IR region, and a large number of terms in the visible and ultraviolet region. Hence, UV spectra properties dominate van der Waals interactions, even though at these frequencies the magnitude of Δ is usually small. Thus, details in the IR region in the ϵ'' spectra need not be as important as those in UV, as far as calculation of Hamaker coefficient goes.³

4.1.3.1 Variation of Hamaker coefficients with temperature

Equation 4-7 can be very misleading, as it suggests a linear variation of Hamaker coefficient with temperature. It is very important to realize that it is not the case. The Hamaker coefficients, for all practical purposes, are independent of temperature. Note that at higher temperatures, the steps of Matsubara frequencies are also higher. In other words, fewer terms will be present in the summation of Equation 4-7 when the temperature is higher, and it somehow always almost balances the $3kT/2$ term outside the summation. As such, the Hamaker coefficients are virtually independent of temperature. The only changes in the Hamaker coefficient with temperature will be due to the change in the ϵ'' spectrum itself with temperature.

This fact is indeed a good news for us, as it essentially says that high temperatures of the order of $1000\text{ }^{\circ}\text{C}$ will infact be beneficial as far as colloidal stability is concerned. And it is certainly easier to make $U_{\text{contact}} \ll kT$ at $1000\text{ }^{\circ}\text{C}$, than it is at room temperature.

4.1.3.2 Effects of changes in ϵ'' spectra in the vdW-Lds spectra

By now, we know that in order to minimize the van der Waals attraction between the particles, their vdW-Lds spectra need to be as close to each other as possible. In the ideal case, when the two vdW-Lds spectra (that of medium and particles) overlap completely, there will be no van der Waals force of interaction between the particles.

It is interesting to determine the variations in van der Waals – London dispersion spectrum with changes in peak positions, peak intensity and peak width in the ϵ'' spectrum.¹¹ In Figure 4-3, ϵ'' spectra of three hypothetical materials are shown with green, blue and red lines. As can be seen, the three spectra are identical in terms of peak positions, but differ in peak height. We then apply

the Kramers-Kronig transformation on these three ϵ'' spectra to obtain the corresponding vdW-Lds spectra for the three materials. As we see, the vdW-Lds spectrum moves up as the peak intensity increases and peak position remains the same.

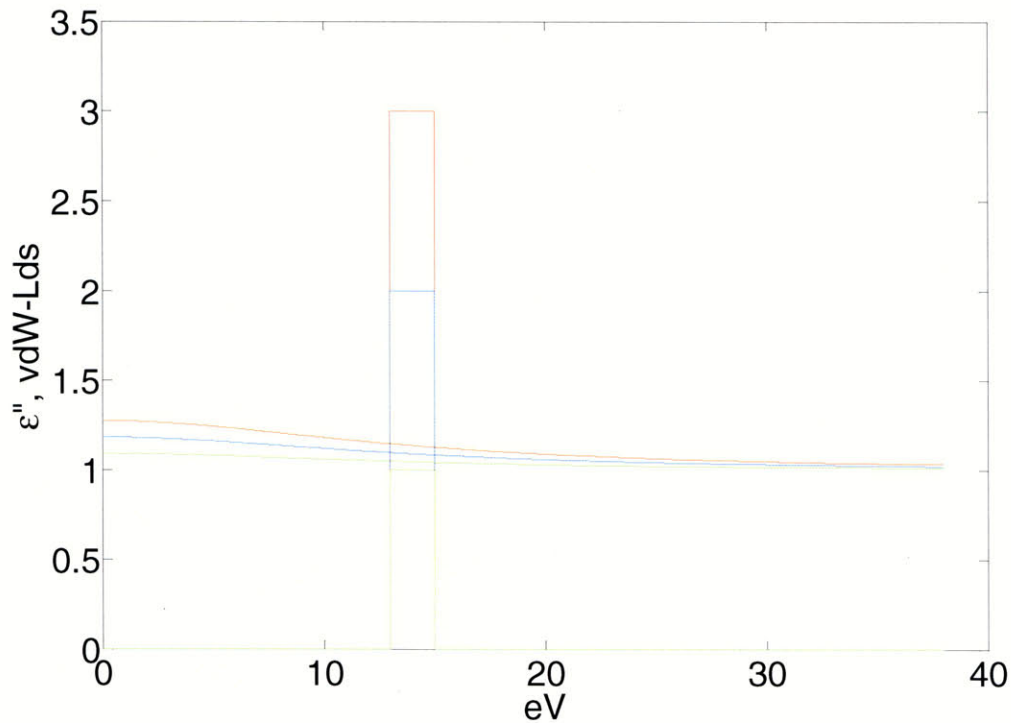


Figure 4-3: Effect of ϵ'' peak intensity on vdW-Lds. As the peak intensity increases, the vdW-Lds shifts upwards.

The variation with peak position is also important. In Figure 4-4, the ϵ'' peak position is varied and intensity is kept the same for three hypothetical materials. As the peak position shifts towards the right, the corresponding vdW-Lds curve flattens out as seen in Figure 4-4.

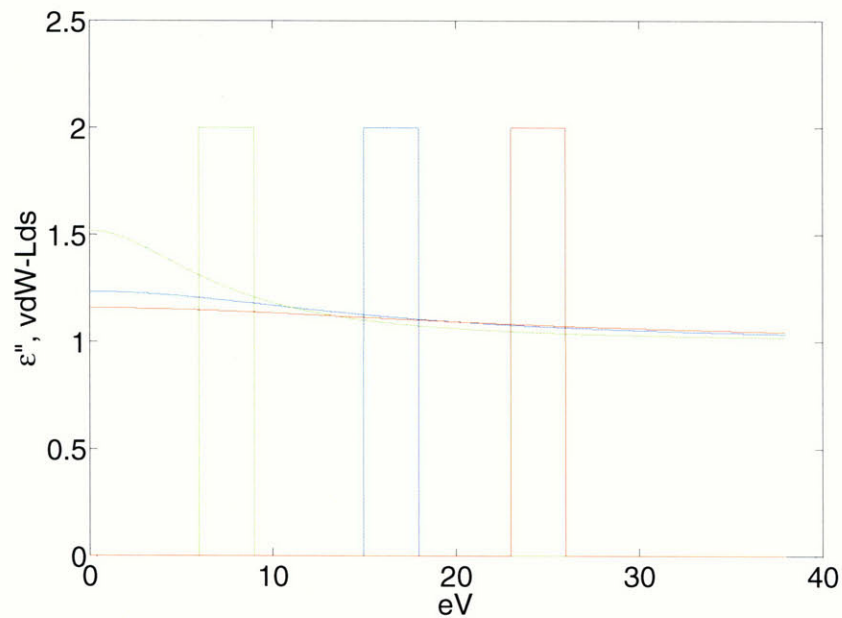


Figure 4-4: Variation of vdW-Lds with ϵ'' peak position. The vdW-Lds flattens out as the ϵ'' peak moves towards right.

Finally, in Figure 4-5, we vary the peak shape, and keep the mean position and area of the three hypothetical materials the same. Interestingly, the three corresponding vdW-Lds curves overlap with one another, which means that shape of the peak does not matter much as far as the van der Waals spectra is concerned provided the peak position and the peak area remain the same.

This result can have some significant implications. Firstly, we expect the ϵ'' spectrum of a crystalline substance to consist of sharp peaks and that of an amorphous or liquid substance to consist of broad and diffuse peaks, but centered at the same position. Figure 4-5 shows us that such mere change of shape will not affect the vdW spectra. Of course, the area under the peak will also be slightly different in a crystalline salt as compared to a molten salt, because the same electrons are occupying a greater volume in molten salt, thereby reducing the electron density in the system. We can make approximate adjustments to this by scaling the solid ϵ'' spectrum such

that the visible index of refraction matches the experimental value of the visible index of refraction of molten salt.

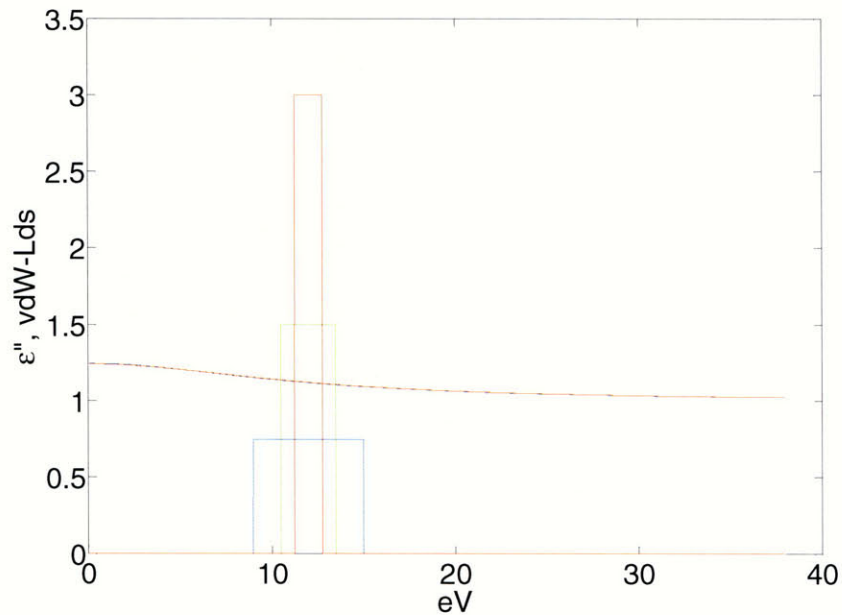


Figure 4-5: Effect of ϵ'' peak width on vdW-Lds with constant peak position and area under the peak

Also, let us take a closer look into how two materials with completely different absorption properties can have a low Hamaker coefficient. Figure 4.6 shows an example of this. Two different materials with absorption peaks in totally different energy ranges have vdW-Lds spectra that are very close to each other. The non-retarded value of the Hamaker coefficient worked out for this particular case is 0.7 zJ. Note that the peak positions and intensities of two different materials can be very different, yet lead to very close van der Waals spectra, and consequently a very low value of the Hamaker coefficient when one material is used as dispersed phase and the other as the medium.

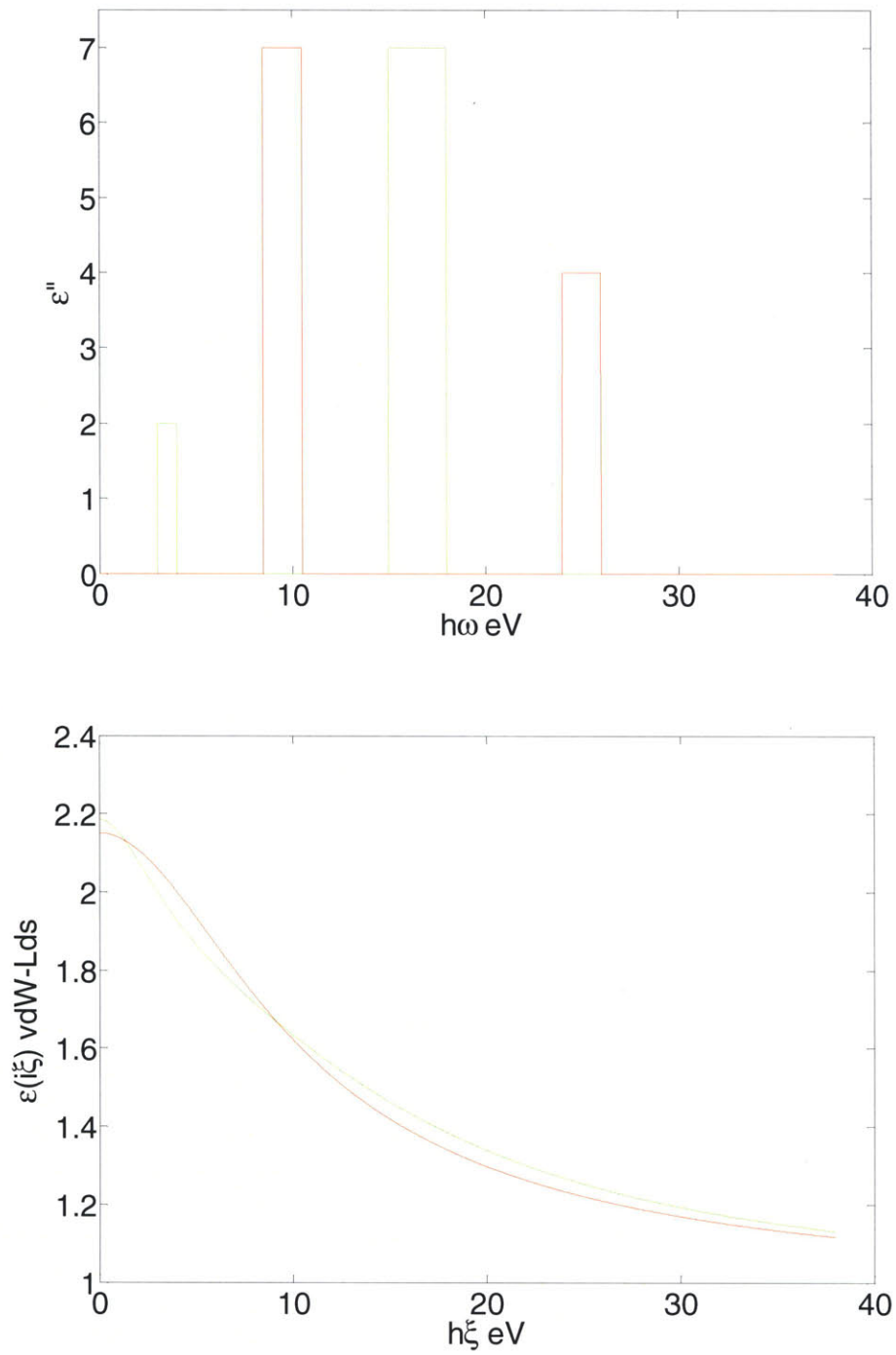


Figure 4-6: The ϵ'' and vdW-Lds spectra of two hypothetical materials, with significantly different absorption properties but very close vdW-Lds

4.1.4 Lifschitz formulation for calculation of Hamaker coefficients

The above formulation, by Hough and White, though generally very accurate is still not the most rigorous one. The Lifschitz formulation used for rigorous calculations of Hamaker coefficient is given below from Equation 4-10 to Equation 4-14.

$$A = \frac{3kT}{2} \sum_{n=0,1,\dots}^{\infty} \int_{r_n}^{\infty} x \ln((1 - \Delta_{12}^2)e^{-x}(1 - \Delta'_{12})e^{-x}) dx \quad (4-10)$$

$$\Delta_{12} = \frac{\varepsilon_1(\xi) - \varepsilon_2(\xi)}{\varepsilon_1(\xi) + \varepsilon_2(\xi)} \quad (4-11)$$

$$\Delta'_{12} = \frac{\mu_1(\xi) - \mu_2(\xi)}{\mu_1(\xi) + \mu_2(\xi)} \quad (4-12)$$

$$\xi_n = \frac{2\pi kT}{\hbar} \quad (4-13)$$

$$r_n = \frac{2l\varepsilon_m^{1/2}\mu_m^{1/3}}{c} \xi_n \quad (4-14)$$

As one can see, the computation of the Hamaker coefficient is fairly involved if the most rigorous form is to be used. However, we still only need the van der Waals spectra of the particles and the medium as an input (provided that the magnetic permeability μ can be ignored, which is the case most of the times). Many systems do not need to use all parts of this complete form and/or certain approximations can safely be made. First, most materials exhibit no or very weak magnetic polarizability and therefore all the $\bar{\Delta}_{ij}$ terms (containing the μ) drop away. Often retardation effects are neglected and instant communication between the interacting materials is assumed. This is equivalent to setting the speed of light variable 'c' to infinity and therefore r_n

goes to zero. At contact/adsorption distances ($l=0$), there is no retardation anyway and thus this assumption is ideal to use in the cases when the particles are in contact. A Taylor series expansion on the integration term is typically done to give an equivalent form that eliminates the logarithmic portions. Since the higher order terms are typically much smaller than the first expansion, the integral can sometimes be eliminated all together. The only exception is for situations of extreme optical contrast (i.e. infinity versus 1). The result of all these approximations and assumptions is the simplified form given by Hough and White, which was stated above in Equation 4-7.

4.2 Obtaining the ϵ'' spectrum for molten salts

Now, in order to compute the van der Waals forces of interactions between the nanoparticles in a molten salt medium, we need to get the van der Waals spectra (and hence the ϵ'' spectra of the particles and the molten salt. These data are already available (or can be easily obtained) for the candidate nanoparticles. However, it is a challenging task to obtain the ϵ'' spectrum for molten salts experimentally due to the high temperatures involved. Ab Initio calculation is the best method to follow, although Ab Initio calculations should not be treated as a substitute for experimental determination of optical properties when feasible. The best method will be to use Ab Initio calculations to determine the ϵ'' spectra till 40 eV and then verify them with experimental results over whatever range is possible. Even a good match of properties (say, the real part of refractive index) in the range of 1.5 to 5 eV will be a strong backing for the results of the Ab Initio calculations.

4.2.1 Experimental options

The experimental technique that can be carried out relatively conveniently for molten salts is Ellipsometry. One has to design a tailor made ellipsometer with a furnace which can handle temperatures as high as 1000°C . Such measurements have been done elsewhere and are certainly possible, but are expensive nevertheless as they require a tailor made equipment. Figure 4-7 shows a set up used to carry out ellipsometric measurements of CaF_2 melt at extremely high temperatures.¹² The apparatus consists of a furnace which encloses the ellipsometer stage, which is able to move freely in the vertical direction.

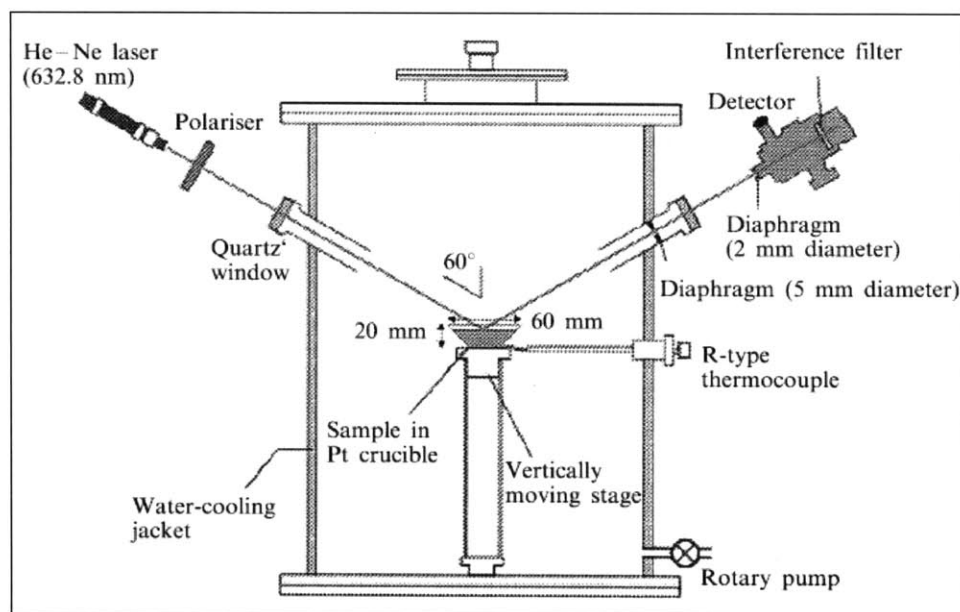


Figure 4-7: Ellipsometric set up for CaF_2 melt at 1823K .¹²

One of the ways to go about building a custom high temperature ellipsometer is to tailor-make a furnace which is dimensionally compatible with the standard commercially available ellipsometers. There are a few important points that need to be taken into account when trying to build such a custom made apparatus. It is important to add optical ports at the correct angles to

allow the ellipsometer to be mounted to the chamber. The key is to allow optical access which will allow our light beam to reach the sample. Then, the surface will reflect light, so it is important that a second window is placed where the specular reflection will reach the other side of the chamber. Such a set up should allow ellipsometric measurements of the molten salts at high temperatures. Thus, cost permitting, it is not that difficult to carry out such high temperature ellipsometric measurements of molten salts, and thereby obtain the van der Waals-London dispersion spectra. In this work, however, we will just stick to the Ab Initio calculations of ϵ'' spectra.

4.2.2. Ab Initio Calculation

As stated above, Ab Initio calculations provide a very good technique to obtain the ϵ'' spectra. However, it is anything but trivial to calculate the ϵ'' spectra of liquid molten salts using Ab Initio calculations. The input that is required for the DFT based quantum calculations is basically all the atoms and the corresponding atomic positions in the lattice. For a crystalline solid, we just need to worry about one unit cell which will repeat itself in space. However, in the case of a liquid or amorphous material, a much larger supercell has to be taken into account because of reduced order. Also, as we saw in section 4.1.3.2, the van der Waals spectra will not be much affected due to the broadening of the peak. Hence, as a starting approximation, the ϵ'' spectra of KCl solid crystals were calculated and were scaled to match the visible refractive index of the molten salts. Thus, the ϵ'' spectra was scaled uniformly across all energies until the corresponding “n – spectra” showed the value reported in the literature for visible wavelengths (generally 589nm). In order to obtain n from ϵ'' , one first needs to apply the Kramers-Kronig transformation on ϵ'' to obtain ϵ' , and then use ϵ' and ϵ'' to obtain n. Figure 4-8 shows the scaled

ϵ'' spectra, the corresponding ϵ' and n spectra, and the vdW-Lds spectrum. Note that the refractive index (n,k) and dielectric constant (ϵ', ϵ'') are related to one another by Equation 4-15.

$$n + ik = (\epsilon' + i\epsilon'')^2 \tag{4-15}$$

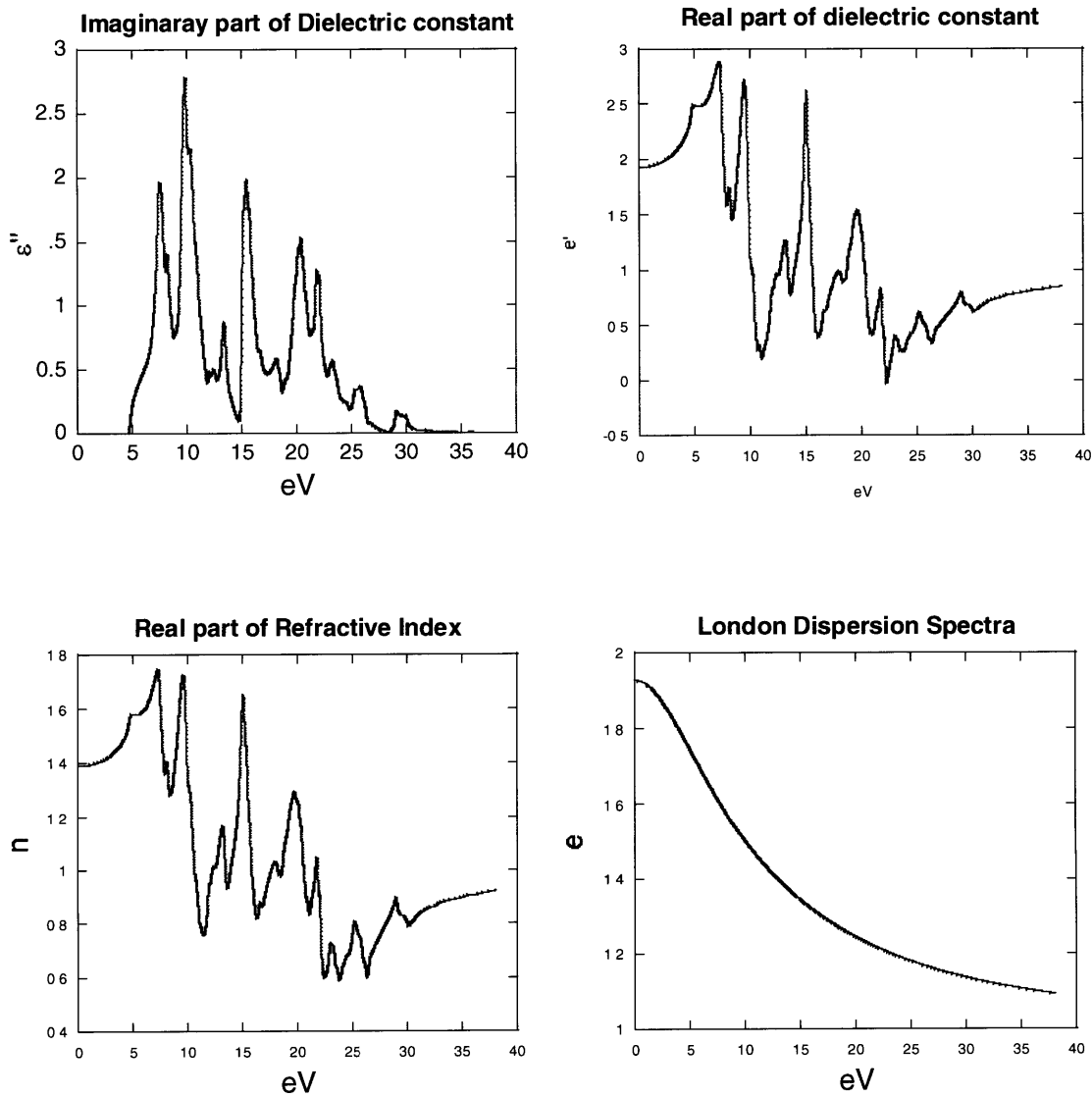


Figure 4-8: The approximated vdW spectra for molten KCl obtained by scaling the ϵ'' spectrum of solid KCl before performing KK transformation.

Thus, the scaled solid KCl van der Waals spectrum is approximated as the molten KCl van der Waals spectrum. While this approximation certainly can be, and has to be improved in future, there is good reason to believe it to be a reasonable starting point

The Hamaker coefficient was then obtained for silica particles in KCl medium using the Lifschitz formulation. The vdW - Lds full spectral data for amorphous silica were taken from the database of Gecko Hamaker, maintained by Prof. Roger French. Figure 4-9 shows the result of the calculation.

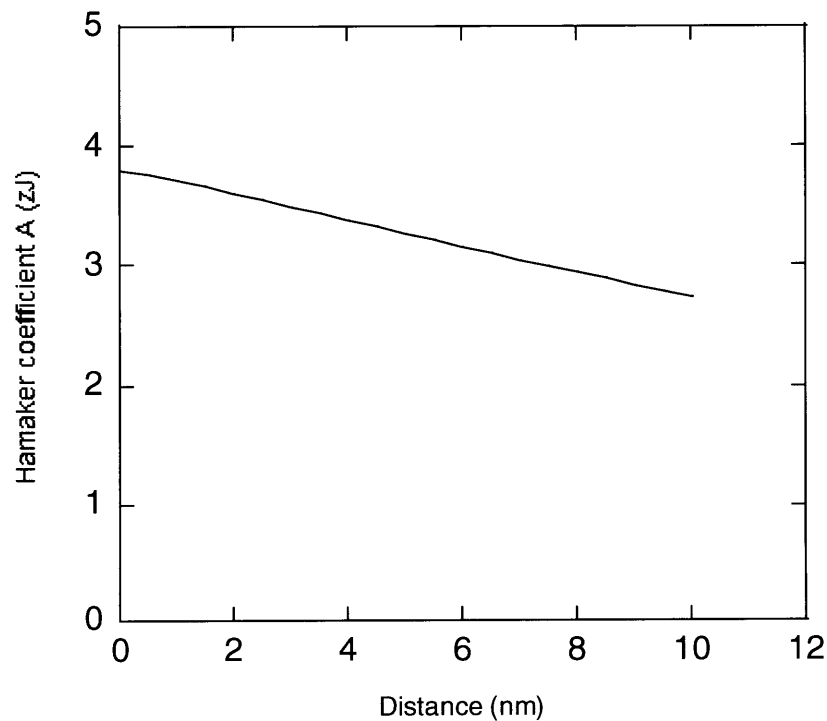


Figure 4-9: Variation of Hamaker coefficient with particle separation for SiO₂-KCl-SiO₂ system. The decreasing value of the Hamaker coefficient with the distance is due to retardation

The effects of retardation can be seen in Figure 4-9, wherein the Hamaker coefficient decreases with increasing distance. Now, $1kT = 13.8zJ$ at 1000K. Thus, the obtained values of the Hamaker coefficient of silica particles are fairly low ($\sim 1/3 kT$), but nowhere close to what we are looking for. However, at this stage we cannot really make a claim on whether the values are low enough for the particles to be kinetically stabilized. As we will see later, evidence suggests that we might need much lower values of the Hamaker coefficient to attain substantial colloidal stability.

4.2.2 Ab Initio calculation of ϵ'' for molten salts

The scaling technique mentioned above is a good starting approximation, but at this time we cannot be sure of the accuracy of the vdW-Lds spectra obtained by this method. Most importantly, we need to be sure whether the change in the ϵ'' spectrum is as we expected (broadening of peaks with the same center position). Hence, we try to refine the model by performing Ab Initio calculations using the structure of molten salt itself. In order to obtain the atomic positions in a molten salt, molecular dynamics simulations were carried out on a 3X3 superlattice of NaCl and KCl at a temperature of 1000 °C and an equilibrating time of 1ns. The superlattice contained on 216 atoms (108 cations and 108 anions), and periodic boundary conditions were applied. The simulations were carried out in a fixed volume ensemble, with the volume of the supercell based on the experimental density of molten NaCl and KCl at 1000 °C. The Born-Huggins-Mayer pair potential was used for the interactions between the ions. The values of the parameters used to describe the pair potential interaction were taken from literature.¹³ The simulation was performed using DL_POLY software.¹⁴

The resultant coordinates of anions and cations at the end of the molecular dynamics simulation were used as input for the Ab Initio calculations. The corresponding ϵ'' , n and the vdW-Lds are shown in the Figure 4-10.

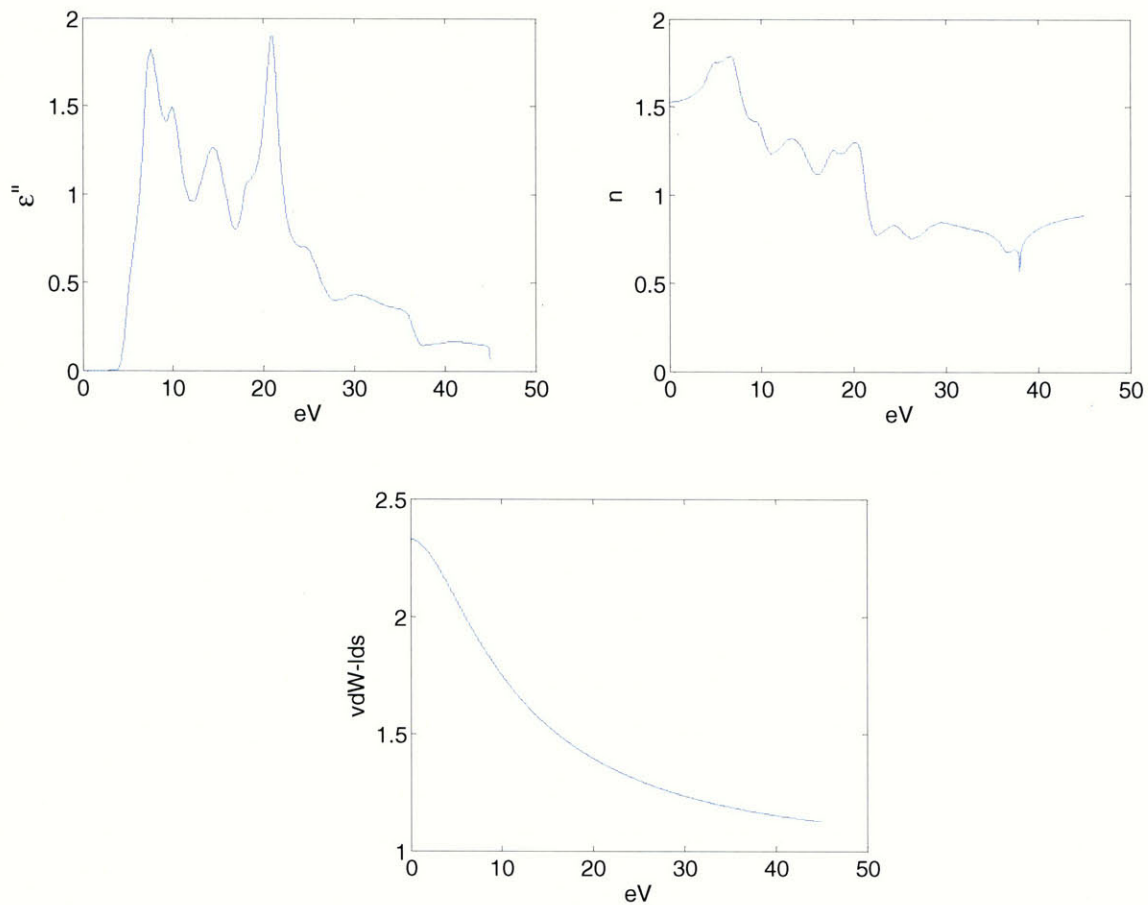


Figure 4-10: The ϵ'' , n and vdW-Lds spectra of molten KCl at 1000°C obtained by Ab Initio calculations using a 3X3 KCl supercell cooked up at 1000 °C.

The results in Figure 4-8 and 4-10 are close, but do not match perfectly. One would normally expect the calculations with molten salt model to be accurate. However the visible index of refraction obtained using the transformation is significantly higher (~ 1.5) than the experimental index of refraction of molten KCl at 1000 °C (1.37). Hence, there is likely to be an error in the resultant vdW-Lds as well. There could be several reasons for this discrepancy. For example, the supercell size could be too small for accurate representation of a molten state. More detailed

study needs to be done before an accurate vdW-Lds can be obtained for molten salts (KCl in this case).

4.3 Summary

In this chapter, we have discovered the detailed theory behind the van der Waals forces of attraction. We have tried to obtain the precise value of Hamaker coefficients of nanoparticles in molten salts and learn how it can be reduced even further. For that, the main challenge is to evaluate the ϵ'' and the vdW-Lds spectra of the system. Using some assumptions, we obtained the vdW-Lds spectrum for molten KCl at 1000°C, using two different methods, and found that the Hamaker coefficient of silica in molten KCl medium is close to 3 zJ. This is a low value of Hamaker coefficient, but not low enough to ensure stability merely on the account of thermal Brownian motion.

A mix and match of various salts can lead to a vdW-spectrum which would be very close to that of an existing material, like silica. Also, nanoparticle materials can be appropriately doped to make their vdW-Lds spectra closely match with one of the molten salt/salt mixtures. However, there is indeed a very long way to go before such salt + nanoparticles systems can be designed, and several difficulties need to be overcome, mainly relating to obtaining accurate data for ϵ'' and vdW-Lds spectra of molten salts.

4.4 References

1. Williams, R. A., Particle Deposition and Aggregation: Measurement, Modelling and Simulation. Butterworth Heinemann: 1995.
2. Israelachvili, J., Intermolecular and surface forces, 2nd edition Academic press, London 1992.
3. Parsegian, V., Van Der Waals forces. Cambridge University Press: New York, 2006.
4. Lifshitz, E. M., The Theory Of Molecular Attractive Forces Between Solids. Soviet Physics JETP-USSR 1956, 2, (1), 73-83.
5. Wooten, F., optical properties of solids. Academic press: New York, London, 1972.
6. Johns, B.; French, R. H.; Kalk, F. D.; McGahan, W. A.; Woollam, J. A., Optical Analysis Of Complex Multilayer Structures Using Multiple Data Types. Optical Interference Coatings, Pts 1 And 2 1994, 2253, 1098-1106.
7. Tan, G. L.; Lemon, M. F.; French, R. H., Optical properties and London dispersion forces of amorphous silica determined by vacuum ultraviolet spectroscopy and spectroscopic ellipsometry. Journal Of The American Ceramic Society 2003, 86, (11), 1885-1892.
8. Ching, W. Y., Theoretical-Studies Of The Electronic-Properties Of Ceramic Materials. Journal Of The American Ceramic Society 1990, 73, (11), 3135-3160.
9. Ching, W. Y.; Gan, F. Q.; Huang, M. Z., Band Theory Of Linear And Nonlinear Susceptibilities Of Some Binary Ionic Insulators. Physical Review B 1995, 52, (3), 1596-1611.
10. Hough, D. B.; White, L. R., The Calculation Of Hamaker Constants From Lifshitz Theory With Applications To Wetting Phenomena. Advances In Colloid And Interface Science 1980, 14, (1), 3-41.
11. Rajter, R. Chirality dependant van der Waals-London dispersion interactions of carbon nanotube systems. Massachusetts Institute of Technology, Cambridge, 2009.
12. Firoz SH, S. T., Endo RK, Susa M, Refractive index measurements of CaF₂ single crystal and melt by ellipsometry. High Temperature-High Pressures 2005, 37, 163-173.
13. Larsen, B., Tormod, F., A Monte Carlo calculation of thermodynamic properties for the liquid NaCl+KCl mixture. Molecular Physics 1973, 26, (6), 1521-1532.
14. [www.ccp5.ac.uk/DL POLY/](http://www.ccp5.ac.uk/DL_POLY/)

5. Conclusions and Future Work

The problem of colloidal stability of nanoparticles in high melting temperature inorganic salts has been explored in some detail. High temperatures and ionicity of the medium make the task of preparing colloidally stable molten salt based nanofluids indeed very challenging. We found out experimentally that settling of nanoparticles in molten salts took place over a matter of few hours. In the first part of the study, we attempted to determine the aggregation kinetics of nanoparticles in molten salts, varying system parameters such as materials of salts and nanoparticles, temperature, concentration of nanoparticles and average size of the nanoparticles. The trends showed that temperature had the most significant impact on the aggregation kinetics. Some of the trends observed could be qualitatively and semi quantitatively explained based on the physical properties of the medium like viscosity and density, and based on the theories of particle deposition and aggregation. We were particularly curious to determine the variation of aggregation kinetics with Hamaker coefficient between the particles, but found out that the effect was minimal, if any. This was because there was no energy barrier to cross for the particles and all collisions would lead to sticking of the particles. Other parameters like temperature, density of the particles etc. often outweighed any effects that might have been due to changes in the Hamaker coefficient.

In the second part of the study, we explored the possibility of stabilizing the nanoparticles by making the Hamaker coefficients ultra low, so that the system could be stabilized merely by the thermal motion of the particles. Although no significant change in aggregation rate was observed for normal Hamaker coefficients, making the Hamaker coefficients low enough such that the thermal energy far outweighs the van der Waals interaction energy between two particles in contact would expectedly lead to long term colloidal stability. In order evaluate such a

possibility, we studied the Lifschitz theory for calculating Hamaker coefficients using the optical properties of the constituent materials over the entire energy range in detail. We found out that, theoretically, it was possible to have significantly different absorption properties and yet have a very low value of Hamaker coefficients. The main challenge in evaluating the Hamaker coefficients between particles in molten salts is evaluating the ϵ'' spectra of the molten salt. Liquid systems at high temperature limits the use of most experimental techniques, and Ab Initio calculations have to be used to estimate the ϵ'' spectra.

In order to engineer the nanoparticles such that the Hamaker coefficient is ultra low, one will need to find appropriate salt mixtures and dopants for the nanoparticles so that the vdW-Lds spectra of the two systems are as close to each other as possible. Clearly, the task is anything but trivial, and much work needs to be done if this area is to be explored in further detail.

Even if engineered nanoparticles could be developed with not very different absorption characteristics, (but ultra-low value of Hamaker coefficients nevertheless), we can make use of core shell morphology to provide high absorption and colloidal stability at the same time. We can have a core with absorption properties very different from that of the salt, and a shell whose vdW-Lds spectrum matches as closely with the salt as possible. This is often referred to as index-matching. The van der Waals interaction between the shells would then be insignificant. At the same time, there would be strong interactions between the cores. However, the steric hindrance provided by the shell would prevent the particle cores from coming close enough to each other, thereby preventing agglomeration and providing stability to the colloidal dispersion. Also, since the two cores are separated by a minimum distance due to the presence of the shell, the actual Hamaker coefficient of their interaction will be much less due to the effects of retardation. This schematic is shown in Figure 5-1.

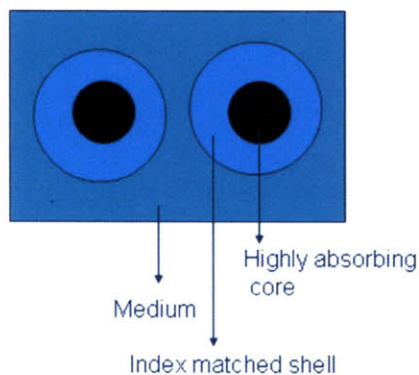


Figure 5-1: Core Shell nanoparticles can provide both strong absorption and colloidal stability

Some other techniques that were not studied in this thesis can also be worth taking a look at. One possibility is to provide steric stability using materials that can withstand high temperatures, like carbon nanotubes. Growing carbon nanotubes on the surface of nanoparticles is likely to present significant challenges as far as processing is concerned, but can surely be one of the ways of taking this problem forward.

In a nutshell, as far as the practical applications that require stable dispersion of nanoparticles are concerned, at the moment it only looks possible if the suspension is periodically agitated by sonication or stirring. On the other hand, nanoparticles present in the system as impurities are not likely to cause any significant alteration in the molten salt characteristics over a long period of time, because they will aggregate and settle in a matter of few hours unless the salt is not stagnant but flowing, or if impurity nanoparticles are generated continuously in the system.